



## Research paper

# Circulating exosomes and gut microbiome induced insulin resistance in mice exposed to intermittent hypoxia: Effects of physical activity



Abdelnaby Khalyfa<sup>a, #, \*</sup>, Aaron Ericsson<sup>b</sup>, Zhuanghong Qiao<sup>a</sup>, Isaac Almendros<sup>c, d, e</sup>, Ramon Farré<sup>c, d, e</sup>, David Gozal<sup>a, #, \*</sup>

<sup>a</sup> Department of Child Health and the Child Health Research Institute, University of Missouri, School of Medicine, Columbia, 400N. Keene Street, Suite 010, MO 65201, United States

<sup>b</sup> University of Missouri Metagenomics Center, Department of Veterinary Pathobiology, College of Veterinary Medicine, University of Missouri at Columbia, Columbia, MO 65201, United States

<sup>c</sup> Unitat de Biofísica i Bioenginyeria, Facultat de Medicina i Ciències de la Salut, Universitat de Barcelona, Barcelona, Spain

<sup>d</sup> CIBER de Enfermedades Respiratorias, Madrid, Spain

<sup>e</sup> Institut d'Investigacions Biomèdiques August Pi Sunyer, Barcelona, Spain

## ARTICLE INFO

## Article History:

Received 1 September 2020

Revised 27 December 2020

Accepted 4 January 2021

Available online 21 January 2021

## Keywords:

Intermittent hypoxia

Exercise

Physical activity

Gut microbiome

Metabolome

OSA

Exosomes

Extracellular vesicles

## ABSTRACT

**Background:** Gut microbiota (GM) contribute to obesity and insulin resistance (IR). Obstructive sleep apnea (OSA), characterized by intermittent hypoxia (IH), promotes IR and alters GM. Since circulating exosomes are implicated in IR, we examined the effects of IH and physical activity (PA) in mice on GM, colonic epithelium permeability, systemic IR, and plasma exosome cargo, and exosome effects on visceral white adipose tissues (vWAT) IR.

**Methods:** C57BL/6 mice were exposed to IH or room air (RA) for 6 weeks with and without PA ( $n = 12/\text{group}$ ), and GM and systemic IR changes were assessed, as well as the effects of plasma exosomes on naïve adipocyte insulin sensitivity. Fecal microbiota transfers (FMT) were performed in naïve mice ( $n = 5/\text{group}$ ), followed by fecal 16S rRNA sequencing, and systemic IR and exosome-induced effects on adipocyte insulin sensitivity were evaluated.

**Findings:** Principal coordinate analysis (PCoA) ordinated revealed B-diversity among IH and FMT recipients that accounted for 64% principal component 1 (PC1) and 12.5% (PC2) of total variance. Dominant microbiota families and genera in IH-exposed and FMT-treated were preserved, and IH-exposed GM and IH-FMT induced increased gut permeability. Plasma exosomes from IH-exposed and IH-FMT mice decreased pAKT/AKT responses to exogenous insulin in adipocytes vs. IH+PA or RA FMT-treated mice ( $p = 0.001$ ).

**Interpretation:** IH exposures mimicking OSA induce changes in GM, increase gut permeability, and alter plasma exosome cargo, the latter inducing adipocyte dysfunction (increased IR). Furthermore, these alterations improved with PA. Thus, IH leads to perturbations of a singular GM-circulating exosome pathway that disrupts adipocyte homeostasis resulting in metabolic dysfunction, as reflected by IR.

**Funding:** This study was supported by grants from the National Institutes of Health grants HL130984 and HL140548 and University of Missouri Tier 2 grant. The study has not received any funding or grants from pharmaceutical or other industrial corporations.

© 2021 The Author(s). Published by Elsevier B.V. This is an open access article under the CC BY-NC-ND license (<http://creativecommons.org/licenses/by-nc-nd/4.0/>)

## 1. Introduction

Obstructive sleep apnea (OSA) is characterized by repetitive upper airway collapse leading to intermittent hypoxia (IH) throughout the sleep period and to recurrent arousals resulting in sleep

fragmentation (SF) [1, 2]. OSA is associated with a large spectrum of neurocognitive, behavioral, cardiovascular, and metabolic adverse consequences, and the disease and its consequences are particularly prominent in obese patients [3, 4], affecting both genders and all ages, albeit differently [5]. Several mechanisms and molecular pathways have been implicated in the altered metabolism elicited by OSA [1, 6]. However, the mechanisms linking OSA, visceral white adipose tissue dysfunction (vWATd), and emergence of IR remain poorly understood, even though the occurrence of oxidative stress and inflammation in OSA is clearly established [3, 7]. Data from animal

\* Corresponding authors.

E-mail addresses: [khalyfa@missouri.edu](mailto:khalyfa@missouri.edu) (A. Khalyfa), [gozald@health.missouri.edu](mailto:gozald@health.missouri.edu) (D. Gozal).

# Equal contributors

## Research in Context

### Evidence before this study

Obstructive sleep apnea (OSA), a condition affecting nearly 1 billion people worldwide, is associated with many adverse consequences, such as systemic hypertension, diabetes mellitus, neurocognitive deficits, and cardiovascular alterations, resulting in significant increments in public health care costs, as well as higher overall mortality rates. Several mechanisms and molecular pathways have been implicated in the metabolic alterations elicited by OSA, and have particularly focused on the effects of intermittent hypoxia (IH) on visceral adipose tissues, and on the emergence of insulin resistance. Parallel work has indicated that the gut microbiome (GM) may play a role in metabolic dysfunction, while evidence points to OSA-induced alterations in GM. Physical activity has a positive effect on energy homeostasis and plays a preventive role against various obesity-related metabolic disorders and against OSA-induced morbidities, while also favorably affecting the GM.

### Added value of this study

In a series of experiments in mice exposed to intermittent hypoxia (IH) mimicking OSA, we show that taxonomic and metabolomic changes in GM increase gut permeability, and lead to alterations in plasma exosome cargo that induce adipocyte dysfunction manifesting as insulin resistance (IR), and such changes were attenuated by physical activity. Fecal microbiota transfers from IH animals to naïve mice promoted emergence of IR (i.e., increases in HOMA-IR) and their plasma exosomes elicited IR on naïve adipocytes. Thus, IH leads to perturbations of a GM-circulating exosome pathway that disrupts adipocyte homeostasis resulting in metabolic dysfunction, as reflected by IR.

### Implications of all the available evidence

We have identified consistent and robust 16S-based taxonomic and metabolomic changes in the GM of mice exposed to IH, and such GM changes promote increased intestinal epithelial permeability that are partially reversed by physical activity. Our findings pave the way for potential exploration of physical activity and pre- and probiotics as adjuvant therapies of OSA and its related morbidities.

is an essential mediator of the interactions between genetics, diet, and physical activity (PA) [19, 20].

Our evolving understanding of how changes in GM composition can promote disease states has prompted interest in developing therapeutic approaches aimed at altering the composition and function of the human microbiota to reverse the disease process of interest [21]. For example, fecal microbiota transfers (FMT) from human healthy non-obese donors to obese patients with IR resulted in improvements in whole-body insulin sensitivity [22, 23]. Our preliminary studies have shown that GM changes occur in rodent models of OSA, i.e., IH or SF [24–27], but the effects of such GM changes on the metabolic dysregulation associated with IH exposures are unknown.

Intercellular communication is an essential hallmark of multicellular organisms and is mediated through direct cell-cell contact or via transfer of secreted vesicles [28–30]. Exosomes are a class of extracellular-vesicles (EVs), 30–120 nm in size, that are released into the extracellular space by reverse budding of multi-vesicular bodies (MVBs) that can bind to the plasma membrane of the acceptor cell and be internalized through either endocytosis or micropinocytosis [2, 29]. Exosomes participate in a vast array of physiological processes such as cell metabolism, proliferation and differentiation [31, 32], and can be isolated from virtually all body fluids [30, 33]. Progress in standardization of exosome isolation and characterization [30, 34, 35] has revealed their critical contributions to many diseases including metabolic and cardiovascular diseases [32, 36, 37]. Plasma-derived exosomes can interact with target tissues and cellular substrates and orchestrate the enrollment of inflammatory cells, altering adipocyte metabolic pathways, and promoting development of IR [36–38]. Among a multitude of cells, adipocytes can take advantage of exosomes by transferring molecules (e.g., miRNAs) that activate metabolic-related pathways, e.g., lipid metabolic pathways [39].

Here, we explored the hypothesis that IH exposures mimicking OSA in young lean mice will induce changes in the GM that increase gut permeability and alter plasma exosome cargo, the latter then inducing vWATd, as illustrated by *in vitro* and *in vivo* IR. Furthermore, we propose that the conglomerate of these alterations would be ameliorated by PA [40]. To this effect, FMT of IH-exposed mice into naïve lean mice were conducted, and the plasma exosome effects on naïve adipocyte insulin sensitivity in recipient mice were evaluated. Our findings indicate that IH leads to perturbations of a GM-circulating exosome pathway that ultimately disrupts adipocyte homeostasis resulting in altered metabolic function, as reflected by IR (Fig. 1a).

## 2. Methods

### 2.1. Animals

All studies were performed under approved protocols from Institutional Animal Care and Use Committee (IACUC), University of Chicago (#7208.3, 2017) and University of Missouri (#9586.1, 2019). Non-obese C57BL/6 male mice 8 weeks of age (Jackson Laboratory, Bar Harbor, Maine, USA) were housed 5/cage at  $24 \pm 1$  °C for 12 h/day light cycle with free access to food and water. Mice were fed ad libitum with standard chow diet. Animals were acclimated to their surroundings for 7 days prior to experiment initiation. At the end of the experiments, mice were euthanized using carbon dioxide (1–2 min) followed by cervical dislocation.

### 2.2. Intermittent hypoxia (IH) and physical activity (PA)

IH was performed according to our standard published protocols [36, 41–43]. Mice were exposed to IH or normoxia (room air, RA) for 6 weeks with and without PA (5 mice/cage) using standard chambers of (Oxycycler A44XO, BioSpherix). The mice were classified as follows: no physical activity (RA, IH), or subjected to physical activity (RA+PA and IH+PA). The pattern of IH consisted of alternating cycles

studies suggest that IH exerts its detrimental effects on glucose metabolism through impairment of pancreatic insulin secretion, as well as direct effects on insulin target organs such as vWAT [8–10]. Several studies have emphasized the physiological roles of gut microbiota (GM) and their metabolites in host homeostatic processes, including immune, metabolic, neurological, and nutritional function [11]. Conversely, alterations in GM are associated with adverse outcomes such as obesity, diabetes, and cancer [12, 13].

Obesity is considered an independent risk factor for cardiovascular diseases (CVDs) [14]. Pediatric obesity contributes to the development of metabolic dysfunction and cardiovascular diseases (CVD) and early mortality in adulthood [15]. Physical activity has been proven as an effective intervention for pediatric obesity, which has a positive impact on blood lipid profiles and blood pressure, as well as on blood levels of metabolic hormones [16–18]. Cumulative evidence suggests that long-term physical activity has a positive effect on energy homeostasis, and plays a preventive role against various obesity-related metabolic disorders, and that the gut microbiome (GM)

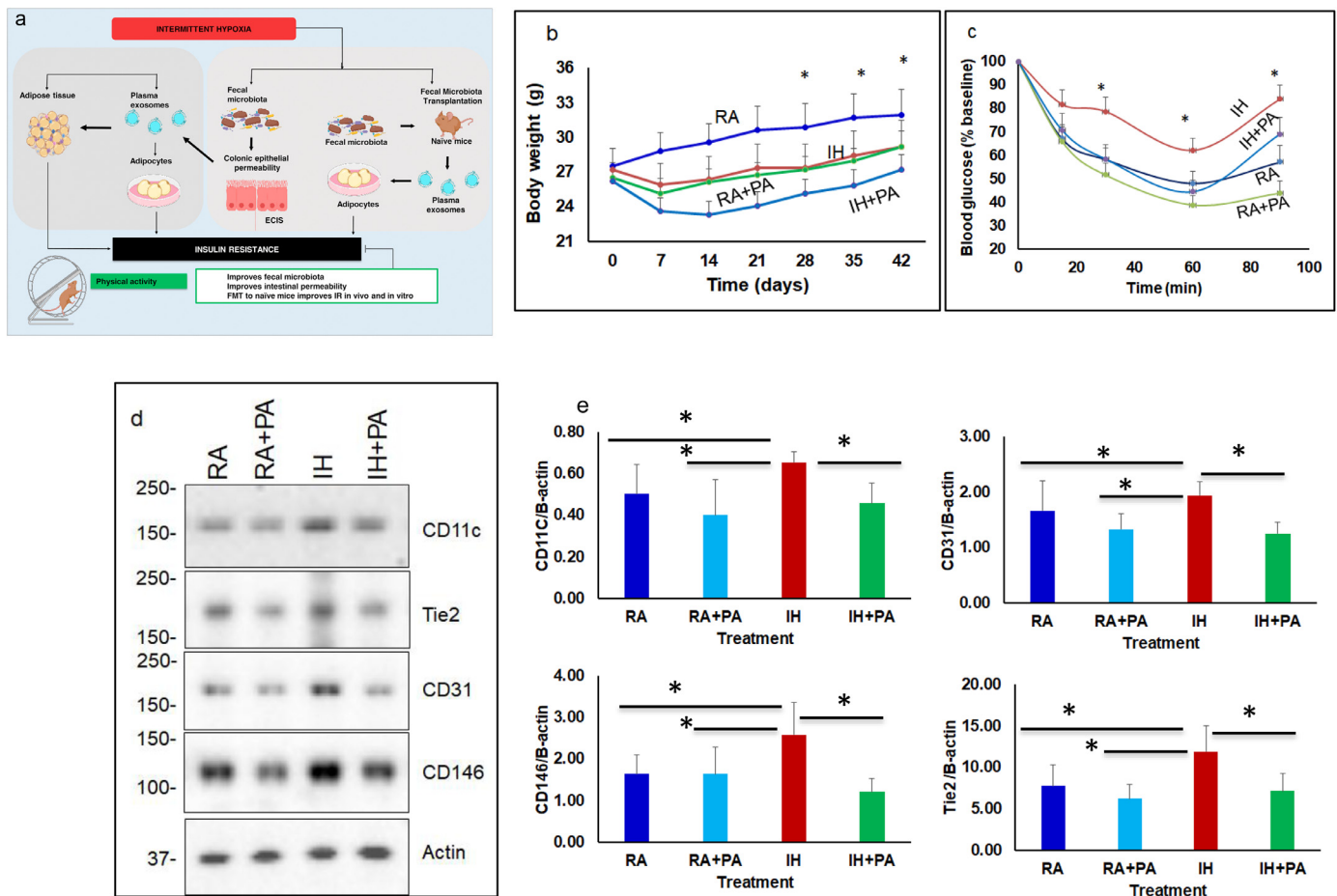


**Fig. 1.** Schematic illustration depicting the effects of chronic intermittent hypoxia (IH) or room air (RA) with and without physical activity in mice. (a) IH induces fecal microbiota alterations that increase colonic epithelial permeability in vivo and in vitro, and elicit changes in functional properties of circulating exosomes that induce insulin resistance. Fecal microbiota transfer of experimental groups recapitulates such findings including the beneficial effects of PA. (b) Average body weight of mice exposed to RA, RA+EX, IH, and IH+PA for 6 weeks with and without exercise (EX) ( $n = 12$ ; \*  $p < 0.01$ ). \* Indicates between IH vs. IH+PA or RA vs. RA+PA. (c) IIT reveals that IH exposures induce insulin resistance compared to RA, and that such effects are improved by PA. (d) Illustrative western blots of vWAT proteins from all 4 experimental groups for CD11c (M1 macrophage), CD146 (integral membrane glycoprotein), CD31 (cell adhesion molecule), and TIE2 (TEK tyrosine kinase). The findings are representative of 8 different experiments. (e) Summary of densitometry signal intensities across experimental groups after normalization to  $\beta$ -actin as the loading control. Significant increases in CD11c protein expression occurred in IH compared to both RA and IH+PA ( $p = 0.01$ ). Results are expressed as fold change and represent mean  $\pm$  SD,  $n = 8$ /group, \* $p = 0.01$ . Two-way of variance (ANOVA) for repeated measures for body weight and IIT: \*\*  $p < 0.01$ ,  $n = 12$ /group. Data are presented as mean  $\pm$  SD. \* Indicates statistical significance between IH vs. IH+PA, and IH vs. RA.

of 90 s (6.5% FiO<sub>2</sub> followed by 21% FiO<sub>2</sub>) for 12 h/day (7:00 AM to 7:00 PM) while RA mice were exposed to 21% FiO<sub>2</sub> throughout. The oxyhemoglobin saturation at the end of the hypoxic period was 68%–75% mimicking values commonly experienced by OSA patients [44].

PA was implemented as previously described [40, 45], using a motorized forced exercise/walking wheel system for mice (Lafayette Instruments, Lafayette, IN). The PA groups were exposed to the walking wheeled system for 30 min, 5 times/week, whereas the control groups were placed in the wheeled system, and remained in the immobile apparatus for the same period of time [45].

### 2.3. Body weight and insulin tolerance test (ITT)

Body weights were measured weekly always at the same time of the day. IIT was performed at the end of each experiment after mice were fasted for 3 h but with water being available ad libitum [46–49].

### 2.4. Fecal microbiota transplantation (FMT) from IH mice into lean mice

Fecal samples from mice exposed to RA or IH with and without PA were collected, and FMTs were performed by oral gavage of a fecal slurry into non-obese naïve mice (C57BL/6, Jackson Labs) as

previously described [50]. Recipient lean mice were fasted for 2 h prior FMT, and the fecal slurry was obtained from mixed fecal pellets originating from 5–6 donor mice. Fecal were suspended by vortexing in 1 mL PBS per 100 mg of feces. Fecal mixtures were centrifugated at 500 g for 5 min, the supernatants were collected for FMT. Each recipient mouse received 100  $\mu$ l of fecal slurry by oral gavage twice/week for 3 weeks in all groups. At the end of this period, feces, plasma and organs were collected for further analyses.

### 2.5. 16S rRNA sequencing

Feces from RA, RA+PA, IH, and IH+PA mice, as well fecal samples from FMT treated mice were processed using PowerFecal kits (Qiagen) according to the manufacturer's instructions [26, 51, 52]. Briefly, bacterial 16S rRNA amplicons were constructed via amplification of the V4 region of the 16S rRNA gene with universal primers (U515F/806R) as previously developed against the V4 region, flanked by Illumina standard adapter sequences [53, 54]. The final amplicon pool was evaluated using the Advanced Analytical Fragment Analyzer automated electrophoresis system, quantified using quant-iT HS dsDNA reagent kits, and further diluted according to Illumina's standard protocol for sequencing on the MiSeq instrument.

Paired DNA sequences were merged using FLASH software [55]. Cutadapt (<https://github.com/marcelm/cutadapt>) was used to remove the primers at both ends of the contig and cull contigs that did not contain both primers. Taxonomy was assigned to selected OTUs using BLAST against the SILVA database v128 of 16S rRNA sequences and taxonomy [56, 57].

## 2.6. Metabolomic profiling

Gut bacterial metabolite profiles and metabolomic analyses were performed with fecal samples as previously described [58]. Briefly, 10 mg of each fecal sample, 1.0 ml of 80% methanol containing 18  $\mu\text{g/ml}$  of umbelliferone (Sigma-Milipore, St. Louis, MO) was added followed by sonication and vortexed for 20 s each. Samples were then shaken in an orbital shaker for 2 h at 140 rpm and centrifuged at 3000 g for 40 mins. Supernatant (0.5 ml) was transferred to an auto-sampler vial for liquid chromatography–mass spectrometry (LC–MS) analysis wherein data was acquired using a Waters Aquity UHPLC system coupled with a Bruker Impact II QTOF mass spectrometer. Data extraction and normalization were performed using Bruker's Metaboscape 4.0 software and statistical analysis (<https://www.bruker.com/products/mass-spectrometry-and-separations/ms-software/metaboscape.html>) and MetaboAnalyst4 software (<https://www.metaboanalyst.ca/>). To each of the remaining sample solutions, 1.5 mL of  $\text{CHCl}_3$  containing 10  $\mu\text{l/ml}$  of docosanol was added, then sonicated and vortexed for 20 s each followed by incubation at 50 °C for 1 hour. One mL of HPLC grade water containing 25  $\mu\text{g/ml}$  of ribitol was added to each sample, sonicated and vortexed for 20 s each and incubated for 1 hour at 50 °C. Sample tubes were centrifuged at 3000 g for 40 mins and allowed to stand for 5 mins. The upper layer non-polar (1 ml) for Gas Chromatography–Mass Spectrometry (GC–MS) non-polar analysis, and another 1 ml solution from the bottom layer for polar GC–MS analysis were transferred to two separate autosampler vials. One pooled sample was prepared each for polar and non-polar GCMS by combining 10  $\mu\text{l}$  of solution drawn from each sample. Dried all the solutions in the autosampler vials using gaseous nitrogen stream. Dried samples for polar GC–MS analysis were methoximated in pyridine with 50  $\mu\text{l}$  of 15 mg/mL methoxyamine hydrochloride, and then trimethylsilylated with 50  $\mu\text{l}$  MSTFA (N-methyl-N-(trimethyl-silyl)trifluoroacetamide) + 1% TMCS (chlorotrimethylsilane) reagent. Samples for non-polar GCMS analysis were reconstituted in 50  $\mu\text{l}$  of pyridine followed by trimethylsilylation with 50  $\mu\text{l}$  of MSTFA+1% TMCS. The derivatized extracts were then analyzed for non-targeted metabolic profiling using an Agilent 6890 GC coupled to a 5973 N MSD mass spectrometer with a scan range from  $m/z$  50 to 650 (Agilent Technologies, Inc., Santa Clara, CA). One  $\mu\text{l}$  of sample was injected into the GC column with a split ratio of 1:5 for polar GC–MS and 1:1 for non-polar GC–MS analysis. Separation was achieved with a temperature program of 80 °C for 2 min, then ramped at 5 °C/min to 315 °C and held at 315 °C for 12 min, a 60 m DB-5MS column (J&W Scientific, 0.25 mm ID, 0.25  $\mu\text{m}$  film thickness) and a constant flow of 1.0 ml/min of helium gas. A standard alkane mix was used for GC–MS quality control and retention index calculations. The data from the pooled sample were deconvoluted using AMDIS and annotated through mass spectral and retention index matching to an in-house constructed spectra library. The unidentified components were then searched and identified using spectral matching to a commercial NIST17 mass spectral library. For the non-targeted ultra-high performance liquid chromatography tandem mass spectrometry (UHPLC–MS/MS) characterization of fecal samples was performed as described in [59–61]. For the UHPLC methods, samples were shaken in an orbital shaker for 2 h at 140 rpm and centrifuged at 3000 g for 40 mins, and 0.5 ml of the supernatant was transferred to an autosampler vial for LCMS analysis wherein data was acquired using a waters aquity UHPLC system coupled with a Bruker Impact II QTOF mass spectrometer. The combined identifications were saved

as an ELU file, and the abundance of the ions in all the other samples were extracted using custom MET-IDEA software. The abundances were then normalized to the internal standard, ribitol, and the normalized values were used for statistical comparisons using Metaboanalyst4 software.

## 2.7. Western blots of visceral white adipose tissues (vWAT)

vWAT samples were homogenized in lysis buffer (50 mM Tris, pH 7.5, 0.4% NP-40, 150 mM NaCl, 10 mg/ml Aprotinin, 20 mg/ml Leupeptin, 10 mM EDTA, 1 mM Sodium orthovanadate, 100 mM Sodium Fluoride). Protein concentrations were measured using the BCA kit (Life Technologies, Grand Island, NY). Equal amounts of total proteins from individual mouse were electrophoresed using SDS-PAGE gel (4–20%) and transferred into a nitrocellulose membrane (Millipore, Billerica, MA). Following the membrane transfer, incubation in blocking buffer (5% nonfat dry milk in 25 mM Tris, pH 7.4, 3.0 mM KCl, 140 mM NaCl, and 0.05% Tween 20 [TBST]) for 1 h at room temperature was performed. Membranes were then incubated overnight at 4 °C with primary polyclonal antibodies recognizing: CD146 (MCAM, Cat# PA5–28,893, RRID:AB\_2,546,369, Thermo Fisher Scientific, Waltham, MA), act as a signal transduction molecule in the recruitment of Fyn kinase, and plays a role in cell adhesion, Invitrogen); CD31 (PECAM-1, Cat# PA5–79,806, RRID:AB\_2,746,921, Thermo Fisher Scientific), is cell adhesion molecule and implicate in trans-endothelial migration of leukocytes and angiogenesis, TIE2, is encodes a receptor that belongs to the protein tyrosine kinase Tie2 family and mediates a signaling pathway that functions in embryonic vascular development (Cat# 05–584, RRID:AB\_309,820, Millipore-Sigma, St. Louis, MO), and CD11c, is transmembrane glycoprotein that forms an  $\alpha/\beta$  heterodimer with CD18 (integrin  $\beta_2$ ) which interacts with a variety of extracellular matrix molecules and cell surface proteins Cat# PA5–79,537, RRID:AB\_2,746,652, Cell Signaling Technology, Danvers, MA), in 1:500 dilutions overnight at 4 °C. Membranes were washed with TBS-T, and incubated with either horseradish peroxidase linked, conjugated  $\beta$ -Actin (Cat# 7074, RRID:AB\_2,099,233, Cell Signaling Technology) for 1 hour at room. Membranes were washed with TBS-T, and incubated with either horseradish peroxidase linked,  $\beta$ -Actin. Immunoreactive bands were visualized using an enhanced chemiluminescence detection system (Chemidoc XRS+; Bio-Rad, Hercules, CA).

## 2.8. Cell cultures

Mouse C57BL/6 primary small intestinal epithelial cells (# C57–6051, RRID not available, Cell Biologics, Chicago, IL) embryonic fibroblasts, pre-adipocytes 3T3-L1 (ATCC® CL-173™, RRID: CVCL\_0123), and RAW 264.7 macrophages (ATCC® CL-173™, RRID: CVCL\_0123; and TIB-71™, RRID:CVCL\_0493) cells were purchased from ATCC (ATCC, Manassas, VA). Mouse primary small intestinal epithelial cells were cultured in a complete epithelial cell medium (#M6621, Cell Biologics, Chicago, IL), while other cells were cultured and maintained in Dulbecco's modified Eagle's medium (DMEM) supplemented with 10% (v/v) bovine serum or fetal bovine serum (Life Technologies, Grand Island, NY), and 100 U/ml penicillin–streptomycin (Life Technologies, Grand Island, NY) in a humidified atmosphere of 5%  $\text{CO}_2$  at 37 °C. Adipocytes were differentiated as described previously in our protocols [36].

## 2.9. Insulin sensitivity in vitro

3T3-L1 ( $5 \times 10^5$ ) cells (ATCC, Manassas, VA) were cultured in DMEM supplemented with 10% FBS and penicillin/streptomycin solution maintained in a humidified incubator at 37 °C and 5%  $\text{CO}_2$  in 24-well plates. After reaching confluence, cells were incubated in differentiation medium containing dexamethasone (2.5  $\mu\text{M}$ ), 3-isobutyl-

1-methylxanthine (0.5 mM), and insulin (10  $\mu\text{g}/\text{mL}$ ). After 4 days, the differentiation medium was replaced with the DMEM medium supplemented with depleted FBS (and the cells were incubated with plasma exosomes isolated from each either mice exposed to RA, RA+PA, IH or IH+PA, or mice treated with FMT for 24 h. Adipocytes were then treated with 0 and 5 nM insulin (Sigma) at 37 °C for 30 min prior to lysis. Cells were washed with PBS, and cells were lysed as described above in Western blots. The supernatants were collected after centrifugation at 15,000 g for 15 min at 4 °C. Protein concentrations of the cell lysates were determined using the BCA Kit (Life Technologies, Grand Island, NY). The lysates were subsequently separated on 12% SDS-acrylamide gel and transferred to nitrocellulose membranes (Millipore, Billerica, MA). After transfer, membranes were incubated in blocking buffer (5% non-fat dry milk in TBST) for 1 h at room temperature. The membranes were then incubated with phosphorylated Akt (Ser473) antibody (Cell Signaling Technology Cat# 9270, RRID:AB\_329,824 y, Danvers, MA, USA) or with total Akt antibody (Cell Signaling Technology Cat# 9272, RRID:AB\_329,827) overnight at 4 °C. Membranes were washed with 25 mM Tris, pH 7.4, 3.0 mM KCl, 140 mM NaCl and 0.05% Tween-20 (TBST), 3 times for 10 min each, further incubated with anti-rabbit immunoglobulin G: HRP-linked antibody (Cell Signaling Technology Cat# 7074, RRID:AB\_2,099,233) in blocking buffer with gentle agitation for 1 h at room temperature. Immunoreactive bands were visualized as described above [36, 51].

#### 2.10. Electric cell-substrate impedance sensing (ECIS)

“Fecal water”, a preparation of water-soluble parts of fecal metabolome, was used to determine barrier disruptive properties of gut microbiota that may underlie endotoxemia. Fecal samples were carefully and gently extracted from mice at the end of each experimental paradigm and were prepared in PBS to a final concentration of 1 mg/ml (w/v), cleared by centrifugation (1 min, 5000 rpm), and filtered using 20  $\mu\text{m}$  membrane filter (Millipore, Bedford, MA). To determine changes in electrical resistance across monolayers of murine primary small intestinal epithelial cells (Cell Biologics, Chicago, IL) ( $5 \times 10^4$  cells), 15  $\mu\text{l}$  per well, (10% (v/v), impedance changes across the cell monolayer were evaluated using an ECIS system (Applied Biophysics, Troy, NY), as previously described [26, 51].

#### 2.11. Exosome characterization and internalization

Exosomes were isolated from plasma and quantified using previously reported experimental approaches in our laboratory [30, 36, 62–66] that strictly adhere to MISEV2018 guidelines [35]. An equal number of exosomes were used for each experiment, and repeat freeze-thaw cycles for plasma and exosomes were avoided.

Morphological evaluation of exosomes was performed using electron microscopy in a subset of exosome fractions and included size distribution and ultrastructural characteristics, as described [30, 64] ( $n = 6–8$  samples per experimental group).

Murine purified exosomes were incubated with Exo-Flow kits (System Biosciences) and analyzed for selective subpopulations of exosome surface markers using flow cytometry (FACSCalibur, BD Biosciences) according to MISEV2018 guidelines [35]. Purified exosomes were incubated with magnetic beads 9.1  $\mu\text{m}$  to CD9, or CD63 for selective capture of distinct subsets of exosomes. Negative experiments were also carried out with all the reagents and beads, but without exosomes [30, 36].

To track exosome uptake and trafficking, exosomes were labeled with PKH26 green fluorescent dye (PKH26 Green Fluorescent Cell Linker Midi Kit for General Cell Membrane Labeling, (Sigma-Aldrich, St. Louis, MO) as per MISEV2018 guidelines [35]. Excess dye from the labeled exosomes was removed through a microspin column G-25 (Sigma-Aldrich). Mouse adipocyte cells were incubated with PKH26-

labeled exosomes, fixed in 4% paraformaldehyde and captured with a Leica SP5 Tandem Scanner Spectral 2-photon confocal microscope (Leica Microsystems, Buffalo Grove, IL) with a 63  $\times$  oil-immersion lens ( $n = 6–8$ ).

#### 2.12. Exosomes and naïve macrophages cells in vitro

The mouse macrophage cell line RAW cells, RAW 264.7, (ATCC® TIB-7) ( $40 \times 10^4$ ) was seeded in 24-well plates in Dulbecco's Modified Eagle Medium (DMEM) supplemented with 10% fetal bovine serum, 1% 100 mM sodium pyruvate, 1% of 10,000 U/mL penicillin and 10,000  $\mu\text{g}/\text{mL}$  streptomycin and maintained in 37 °C humidified incubator containing 5% CO<sub>2</sub>. After reaching confluence, cell medium was replaced with 10% depleted FBS (exosome-depleted FBS media supplement (SBI, Palo Alto, CA) in DMEM, and the cells were incubated with plasma exosomes derived from experimental groups and incubated at 37 °C, 5% CO<sub>2</sub> for 24 h. Further, cells were stained with fluorescence conjugate-primary antibodies (F4/80-PE/Cy7: Cat# 123,114, and CD11c-APC: Cat#117,310, Biolegend, San Diego, CA) in staining buffer (1% BSA in PBS) at 4 °C for 30 min. After washed twice cells were analyzed with a flow cytometer (Canto II; BD Biosciences, San Jose, CA), and data analysis was performed using the FlowJo software (Tree Star, Ashland, OR).

#### 2.13. FMT and intestinal permeability assay

FITC-dextran (4-kDa; Sigma-Aldrich St. Louis, MO) was utilized for assessment of intestinal permeability assay in lean mice (C57BL/6) gavaged with FMT derived from mice exposed to RA or IH for 6 wks. Mice were fasted for 4 h, and about 50  $\mu\text{l}$  of blood were collected from the tail vein as time zero. FITC dextran was prepared in FITC dextran of 80 mg/mL phosphate-buffered saline (PBS) buffer and 150  $\mu\text{l}$  was gavaged to each mouse ( $n = 8$ ). Blood samples were collected following gavaged dextran for up to 4 h. Plasma was obtained after centrifugation at 2000 g for 5 min, and further plasma was diluted 1:10 (v/v) in PBS for the 4-kDa FITC dextran analyses. Fluorescence was measured spectrophotometrically Photomultiplier Tube detection system (GloMax-Multi Detection System; Promega, Madison, WI) in 96-well plates (excitation: 485 nm, emission: 528 nm). Readings of relative fluorescence units was measured in duplicate and averaged. Permeability was expressed as relative fluorescence units between the groups being compared.

#### 2.14. Statistical analysis

Univariate data (e.g., read counts, richness or  $\alpha$ -diversity of individual samples) were first tested for normality using the Shapiro-Wilk method, and equal variance using the Brown-Forsyth method. Normally and non-normally distributed data were then tested for differences using two-way analysis of variance (ANOVA) or Kruskal-Wallis one-way ANOVA on ranks, respectively, with RA vs. IH, and PA vs. no PA as factors. Correlations between univariate data were performed using Spearman's rank order correlation. Testing described above was performed using Sigma-Plot 14.0 (Systat Software). Testing for differences in multivariate data (e.g.,  $\beta$ -diversity between groups) was performed using two-way permutational multivariate analysis of variance (PERMANOVA), performed using Past software [67]. For all such comparisons, both Jaccard (unweighted) and Bray-Curtis (weighted) similarities were used. Two-tailed p-values were calculated for all pairwise multiple comparison procedures using the Student-Newman-Keuls test among groups. Multivariate statistical analyses such as PLS-DA, ANOVA, box plots, and volcano plots were performed with the MetaboAnalyst 3.0 program after data pre-treatments, i.e., normalization to the sum, log transformation and Pareto scaling (<http://www.metaboanalyst.ca/>). Data are presented as mean

± SD. A two-tailed p-value <0.05 was considered as statistically significant.

### 2.15. Role of the funding source

The funders had no role in the study design, data collection, data analysis, interpretation, or writing of report.

## 3. Results

### 3.1. IH induces systemic alterations in lean mice

Mice exposed to IH exhibited lower body weights (BW) compared to RA mice ( $p = 0.001$ ;  $n = 12$ /group), while mice exposed to IH had higher BW vs. IH+PA ( $p = 0.02$ ;  $n = 12$ /group). In contrast, BW in RA+PA was lower vs. RA [ $p = 0.01$ ,  $n = 12$ /group (Two-way of variance (ANOVA); Fig. 1b)].

Mice exposed to IH exhibited altered responses to insulin vs. RA;  $p < 0.01$ , and such effects were attenuated by EX (IH vs. IH+PA;  $p = 0.01$  (Two-way of variance (ANOVA) for repeated measurement), Fig. 1c), indicating that IH induces systemic IR.

An evaluation of several markers of inflammation (Fig. 1d), revealed that mice exposed to IH exhibited increased CD11c expression in vWAT compared with IH+PA (Fig. 1d;  $n = 8$ /group;  $p = 0.031$ ), (Two-way of variance (ANOVA). Furthermore, western blots for other macrophage and endothelium-associated proteins including CD31, CD146, and TIE2 showed significant increases in expression in IH compared to IH+PA or RA, indicating that IH may enhance vascularization and the recruitment of inflammatory cells in vWAT, and that PA attenuates these effects (Fig. 1d and 1e).

### 3.2. Effect of fecal microbiome on small intestinal epithelial cells barrier disruption

Cells were exposed to fecal water from all exposed groups, and trans-monolayer resistance was significantly disrupted by IH-associated fecal metabolites when compared to IH+PA ( $p < 0.004$ ). However, both IH conditions increased permeability of the monolayer barrier when compared to RA and RA+PA, ( $p = 0.003$ ,  $n = 12$ /group (Two-way of variance (ANOVA), Fig. 2a and 2b), suggesting a differential effect on epithelial permeability via IH-induced changes in the gut microbiome and metabolome.

### 3.3. IH and PA associated with changes in gut microbiota

Significant exercise-dependent increases in richness (Fig. 3a) and  $\alpha$ -diversity (Fig. 3b) (two-way ANOVA with *post hoc* comparisons using Holm-Sidak method) were detected. At the level of phylum, significant exercise-dependent increases in the *Firmicutes* to *Bacteroidetes* ratio were detected in RA-exposed mice (Fig. 3c), while IH was associated with increases and decreases in the phyla *Patensibacteria* ( $p < 0.001$ ,  $F = 15.27$ ) and *Tenericutes* ( $p < 0.001$ ,  $F = 38.4$ ), respectively.

At a finer taxonomic level (Fig. 3d), significant IH-dependent differences in the relative abundance of 29 operational taxonomic units (OTUs) were detected (one-way permutational multivariate analysis of variance (PERMANOVA) (Supplementary Table 1). Taxa present at greater abundance in IH-exposed mice were largely within the phylum *Bacteroidetes*, with the exception of two *Lactobacillus* spp., two  $\alpha$ -*Proteobacteria*, and *Candidatus Saccharimonas*, while taxa at greater abundance in RA-exposed mice were predominantly within the phylum *Firmicutes* including three different strains of *Eubacterium* spp., and several other members of the families *Ruminococcaceae* and *Lachnospiraceae*. Regarding EX-associated differences, 21 of 33 OTUs were at greater abundance in samples from exercised mice, including mainly *Firmicutes*, plus one OTU each from the

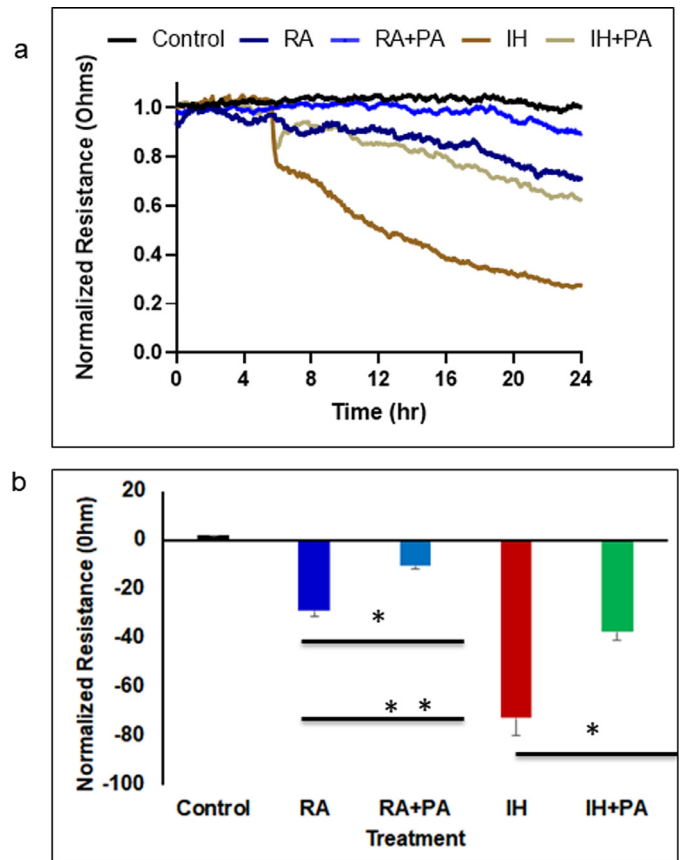


**Fig. 2.** Fecal water derived from mice exposed to IH or RA for 6 weeks with and without PA was added to monolayers of mouse intestinal epithelial cells, and changes in resistance were evaluated using Electric Cell-substrate Impedance Sensing (ECIS). (a) Mean changes in normalized resistance across the mouse intestinal epithelial cells monolayer over time after fecal water treatment at time 0. (b) Mean mouse intestinal epithelial cells monolayer resistance changes after 24 h of exposure to fecal water from each experimental group. Data are presented as mean ± SD;  $n = 12$ /experimental condition, \*  $p = 0.003$ , \*\*  $p = 0.0001$ . Two-way of variance (ANOVA) for non-repeated measures was used. Control indicates cells without fecal water.

*Actinobacteria* and *Bacteroidetes* phyla. Similarly, of those 12 OTUs (36.4%) that were at a lower relative abundance in samples from exercised mice, nine were from the *Bacteroidetes*. Thus, IH was associated with increased abundance of *Bacteroidetes* and  $\alpha$ -*Proteobacteria*, and decreased abundance of Gram-positive *Firmicutes*. Furthermore, PA was associated with increased abundance of many of the same OTUs found to be reduced in IH-exposed mice.

Comparisons of  $\beta$ -diversity via ordination revealed significant effects of IH ( $p = 0.0001$ ,  $F = 13.7$ ) and exercise ( $p = 0.0001$ ,  $F = 10.4$ ) (one-way permutational multivariate analysis of variance (PERMANOVA) (Fig. 3e), mirrored by a hierarchical clustering approach (Fig. 3f).

### 3.4. Fecal metabolome

Principal component analysis (PCA) based on the LCMS analysis of the fecal metabolome resulted in the detection of 1858 compounds, which clearly differentiated the samples based on exposure to IH, with minimal distinction based on PA (Fig. 4a). Serial ANOVA of these compounds detected IH-dependent differences in the abundance of 25 compounds (Supplementary Table 2). Serial ANOVA of the 1858 compounds detected via LCMS detected IH-dependent differences in the abundance of 28 compounds (3 of the 28 likely being duplicates of the same metabolite) after correction for multiple tests (Supplementary Table 2). Thus, of the 25 distinct compounds found to differ in association with IH, 21 were at a greater abundance in IH-exposed

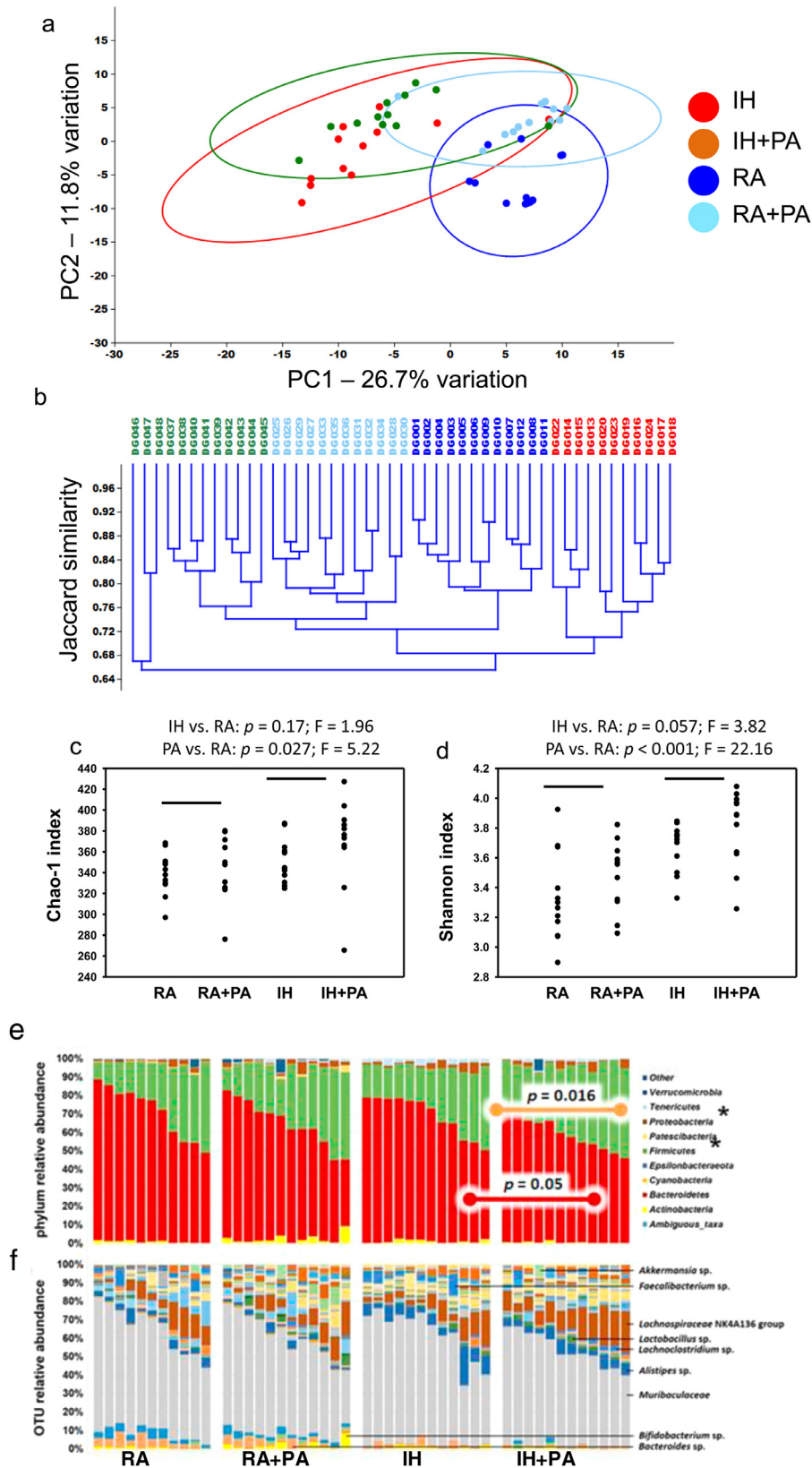


**Fig. 3.** Principal component analysis, hierarchical clustering, dot plots and stacked bar charts for 16S RNA analyses of fecal samples obtained from mice exposed to IH, RA for 6 weeks with and without PA. (a) Principal component analysis, and (b)  $\alpha$ -diversity in feces of wild-type mice exposed to RA or IH in the presence or absence of PA,  $p < 0.05$  differences between groups (two-way ANOVA with *post hoc* comparisons using Holm-Sidak method). (c) Stacked bar charts showing the taxonomic distribution of samples within each group at the level of phylum (IH vs. RA:  $p = 0.17$ ;  $F = 1.96$ ; PA vs. ctl:  $p = 0.027$ ;  $F = 5.22$ ), (d) and operational taxonomic unit with prominent taxa labeled (IH vs. RA:  $p = 0.057$ ;  $F = 3.82$ ; PA vs. ctl:  $p < 0.001$ ;  $F = 22.16$ ). (e) Principal component analysis, (f) hierarchical clustering according to the unweighted pair group method with arithmetic mean (UPGMA) using Jaccard similarities, to visualize the relationship between the fecal microbiota of mice exposed to different conditions,  $n = 12$ /group. Statistical comparisons in PCoA were made using one-way permutational multivariate analysis of variance (PERMANOVA).

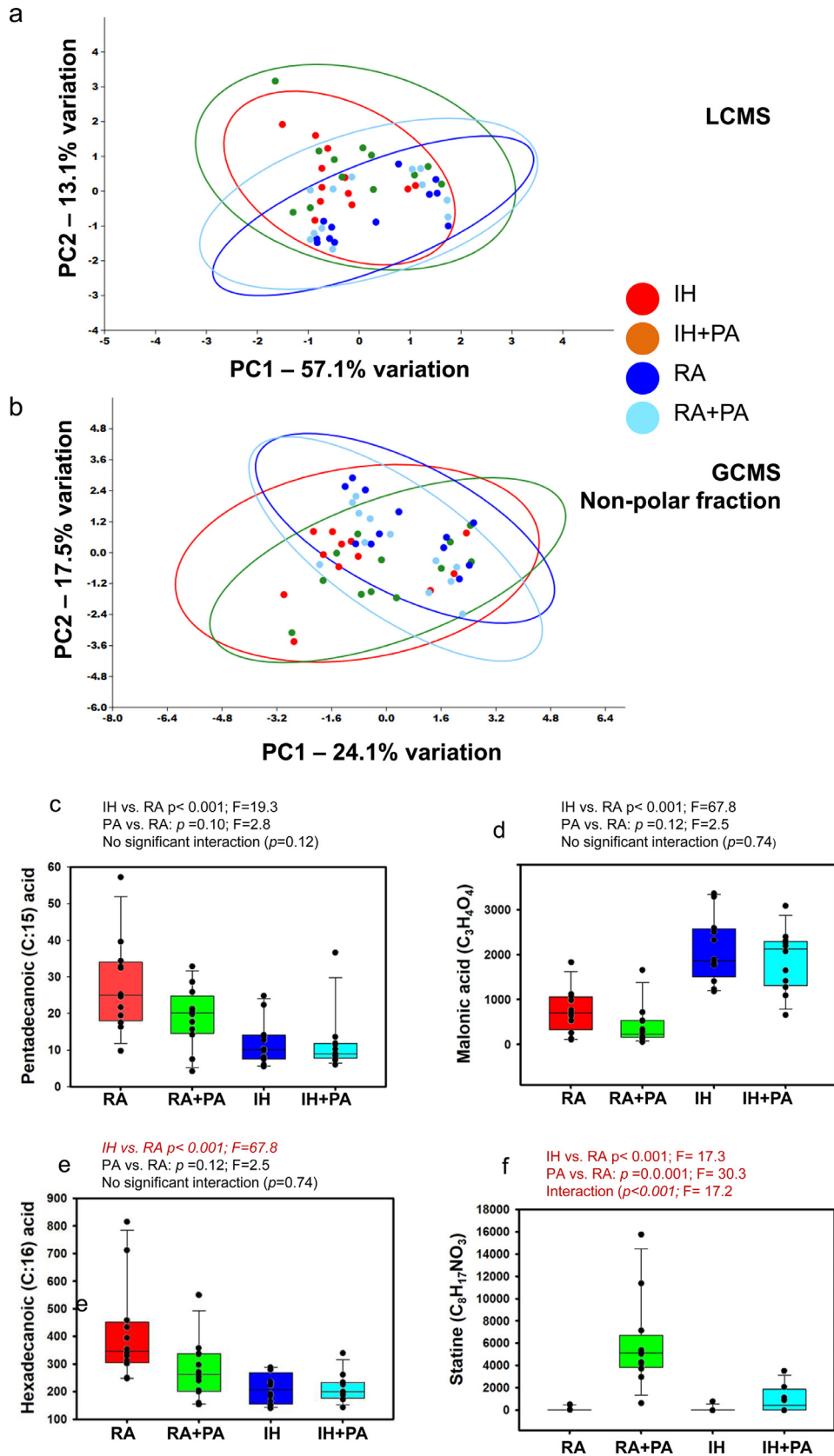


**Fig. 4.** Principal component analysis and Tukey box plots for fecal metabolome in mice exposed to RA and IH for 6 weeks with and without PA. (a) Principal component analysis of the fecal metabolome identified via ultra-high-pressure liquid chromatography-mass spectroscopy (UHPLC-MS). (b) Gas chromatography-mass spectroscopy, nonpolar. (c) Tukey box plots showing the abundance of Pentadecanoic acid (C15:0); IH vs. RA:  $p < 0.001$ ;  $F = 19.3$ ; PA vs. RA:  $p = 0.10$ ;  $F = 2.8$ ; no significant interaction ( $p = 0.12$ ), (d) Hexadecanoic acid (C17:0); IH vs. RA:  $p < 0.01$ ;  $F = 17.5$ ; PA vs. RA:  $p = 0.049$ ;  $F = 4.1$ ; interaction:  $p = 0.04$ ;  $F = 4.5$ , (e) Malonic acid (C<sub>3</sub>H<sub>4</sub>O<sub>4</sub>); IH vs. RA:  $p < 0.001$ ;  $F = 67.8$ ; PA vs. RA:  $p = 0.12$ ;  $F = 2.5$ ; no significant interaction;  $p = 0.74$ ), and (f) Statine (C<sub>8</sub>H<sub>17</sub>NO<sub>3</sub>); IH vs. RA:  $p < 0.001$ ;  $F = 17.3$ ; PA vs. RA:  $p < 0.001$ ;  $F = 30.3$ ; interaction:  $p < 0.001$ ;  $F = 17.2$ . Statistical analyses indicate main effects of each factor and interaction, based on two-factor ANOVA,  $n = 12$ /group.

mice (84%), while only 4 of 25 (16%) compounds were in greater abundance in RA-exposed controls. Thus, the primary differences between all four treatment groups in the LCMS data represent compounds that were elevated in association with IH (9/12), and which were either normalized to control levels with PA (5/12), or remained at an increased level despite PA (4/12).

In parallel, GC–MS was used to profile the nonpolar and polar volatile fractions of the fecal samples. Principal component analysis (PCA) based on the nonpolar metabolome identified via GC–MS revealed clear IH-dependent separation of samples (Fig. 4B), while no clustering was observed when samples were ordinated using the polar fraction (data not shown). Of the 238 compounds identified via GC–MS in the nonpolar fraction, treatment-dependent differences in 22 compounds (Supplementary Table 3) all represented IH-dependent increases. Of the 62 compounds identified in the polar fraction, only five significant differences were detected, all representing IH-dependent decreases (Supplementary Table 4). The nature of those compounds detected at increased levels in feces from IH-exposed mice included smaller molecules such as adenine (C<sub>5</sub>H<sub>5</sub>N<sub>5</sub>) and statine (C<sub>5</sub>H<sub>5</sub>N<sub>5</sub>), a  $\gamma$ -amino acid found in the sequence for the protease inhibitor pepstatin, as well as several extremely long carbon-chain compounds ranging up to a C:64 backbone (C<sub>64</sub>H<sub>101</sub>N<sub>7</sub>O<sub>30</sub>P<sub>2</sub>). Tukey box plots showing the abundance of Pentadecanoic acid (C15:0) (Fig. 4c); Hexadecanoic acid (C17:0) (Fig. 4d); Malonic acid (C<sub>3</sub>H<sub>4</sub>O<sub>4</sub>) (Fig. 4e); and Statine (C<sub>8</sub>H<sub>17</sub>NO<sub>3</sub>) (Fig. 4f). Statistical analyses indicate main effects of each factor and interaction, based on two-factor ANOVA,  $n = 12$ /group.

### 3.5. FMT in naïve mice

To isolate the GM-mediated effects of IH from other systemic effects, feces from RA, IH and IH+PA-exposed donor mice were transferred to naïve recipient mice via FMT. Comparison of GM in donor mice exposed to RA, IH, or IH-PA, and in FMT recipient mice indicated successful transfer of the GM. Specifically, IH-dependent increases in richness (Supplementary Figure S1A) and  $\alpha$ -diversity (Fig. S1b) were

present in corresponding FMT recipients, and PCA revealed tight clustering of donor and cognate FMT recipients and clear separation of samples based primarily on exposure to IH (Fig. S1c and d).

### 3.6. Effect of exosomes from IH-exposed mice on insulin sensitivity and macrophages in vitro

Exosome isolation, quantification, and exosome uptake were performed as previously described (Fig. Supplementary figures 2 and 3) [30, 36]. To evaluate in vitro the effects of plasma exosomes derived from all four treatment groups on insulin sensitivity, differentiated adipocytes (3T3-L1) were treated with equal numbers of exosomes (30  $\mu$ g) for 24 h in the presence of depleted FBS, and then treated with 5 or 0 nM insulin, after which AKT phosphorylation was appraised using western blots. The increases in the expression of pAKT relative to total AKT expression elicited by insulin treatment were significantly attenuated in IH compared to IH+PA (Fig. 5a and b). No significant differences emerged between RA and RA+PA. In addition to the effects of exosomes on naïve adipocytes, we also studied their effects on naïve macrophages (Fig. 5c). IH-derived exosomes shifted macrophage polarity toward M1 (CD11c positivity; vs. RA:  $p = 0.029$ ;  $n = 6$ /group), and such effect was reduced in IH+PA vs. IH:  $p = 0.041$ ;  $n = 6$ /group) with no significant differences between RA vs. RA+PA ( $n = 6$ /group), (Two-way ANOVA).

### 3.7. FMT, plasma exosomes, and adipocyte and systemic insulin sensitivity

FMT-recipients from IH donors demonstrated significant increases in IR compared to FMT-recipients from FMT+IH+PA or RA donors (FMT+IH:  $3.58 \pm 0.81$ ; FMT+IH+PA:  $2.71 \pm 0.34$ ; IH vs IH-PA  $p = 0.008$ ; RA:  $1.98 \pm 0.29$ ; RA vs. IH:  $p = 0.002$ ), (Two-way ANOVA), therefore recapitulating the same effects of IH in mice that were not exposed to the IH paradigm. These data suggest that the effect of IH on IR is mediated by the GM.

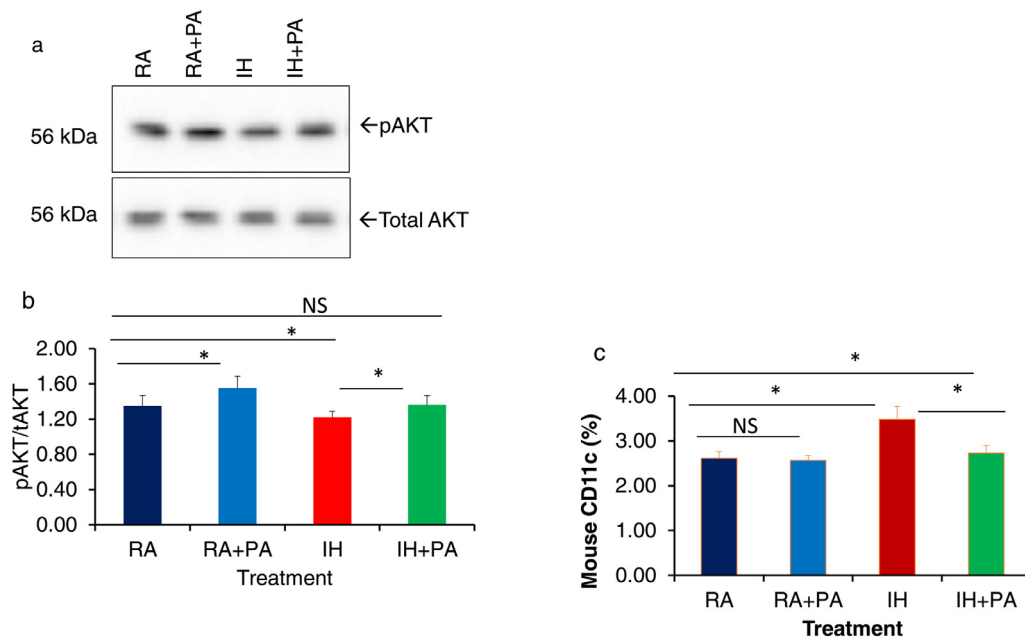


**Fig. 5.** Effects on insulin sensitivity on naïve adipocytes by plasma exosomes derived from mice exposed to IH or RA for 6 weeks with and without PA. (a) Representative Western blots of pAKT and tAKT after treatment with plasma exosomes followed by 5 nM of exogenous insulin for 30 min. (b) Mean pAKT/tAKT ratios,  $n = 8$  per experimental conditions. (c) Effects of plasma exosomes on CD11c expression by naïve macrophage (RAW 264.7) cells using flow cytometry. An equal number of exosomes ( $20 \times 10^6$ ) was used from each condition. \* Indicates statistical significance of IH vs. IH+PA,  $p < 0.05$ ,  $n = 8$ /condition. Two-way of variance (ANOVA) for non-repeated measures was used. NS indicates not significant.

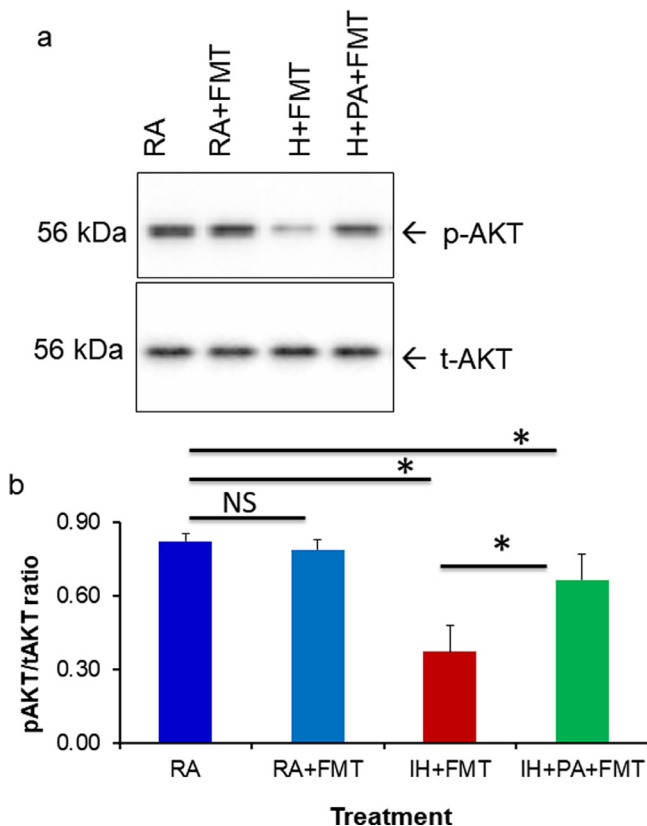


**Fig. 6.** Effects of fecal microbiota transplantation (FMT) on insulin sensitivity in vitro. FMT using fecal slurry from mice exposed to IH or RA for 6 weeks with and without PA were performed for 3 weeks in recipient naïve mice, and plasma samples were then collected from which exosomes were isolated. Equal number of exosomes ( $20 \times 10^6$ ) were applied in vitro to naïve adipocyte (3T3-L1) cells for 24 hrs, after which insulin sensitivity was examined by adding insulin 5 nM for 30 min. (a) Representative Western blot of pAKT and tAKT from adipocytes after exosome and insulin treatment ( $n = 5$  per experimental condition). (b) Mean pAKT/tAKT ratios in naïve murine adipocytes (3T3-L1) treated with exosomes from FMT recipients showing reduced insulin sensitivity in FMT-IH vs. all other groups ( $n = 5$  per experimental condition). Two-way of variance (ANOVA) for non-repeated measures was used. \*Indicates,  $p < 0.05$ . NS indicates not significant.

We also examined the effects of plasma exosomes derived from mice receiving FMT on naïve adipocytes. Similar to the effects of plasma exosomes obtained from mice exposed to IH, significant reductions in phosphorylated-AKT (pAKT)/total AKT (tAKT) ratios occurred in FMT+IH group compared to FMT+IH+PA ( $p = 0.001$ ,  $n = 5$ ), and FMT-RA ( $p < 0.001$ ;  $n = 6$ ), (Two-way ANOVA), while no significant differences were detected in the effects of exosomes from FMT+RA vs. RA group (Fig. 6a and b), suggesting that FMT from IH mice induced insulin resistance in naïve lean mice that were never exposed to IH. The influence of IH on IR, mediated through the GM, is also reliant on IH-induced changes in plasma exosomes.

### 3.8. FMT and permeability assay

Lastly, FMT-recipients from IH donors (FMT+IH) demonstrated significantly greater intestinal permeability compared to FMT-recipients from RA donors ( $p = 0.003$ ,  $n = 8$ ), Two-way ANOVA), when measured using an in vivo dextran-FITC assay (Fig. S4). Collectively, these results indicate that the IH-mediated effects on IR are dependent on changes in the composition and function of the GM in the context of disrupted barrier function, and concurrent changes in the plasma exosome cargo content.

## 4. Discussion

In this study, we have identified consistent and robust 16S-based taxonomic and metabolomic changes in the GM of mice exposed to IH, and that such changes promote increased intestinal epithelial permeability that are partially reversed by physical activity. In parallel, we have also recapitulated our previous findings and those of others that chronic IH exposures foster the emergence of systemic IR and inflammation in vWAT, and now show for the first time that such changes can be attenuated by regular physical activity. Furthermore, we show that exosomes from lean mice exposed to IH and RA induce IR in naïve adipocytes and promote M1 polarization in naïve macrophages in vitro, and that PA minimizes the functional properties of exosomal cargo. Finally, as a proof of concept that the effects of IH may be mediated, at least in part, by a GM-plasma exosomal pathway, we conducted FMT experiments, and found that naïve mice whose GM was modified to resemble the IH-induced GM changes but without exposures to IH, displayed reductions in insulin sensitivity (i.e., increases in HOMA-IR) and harbored plasma exosomes that elicited IR on naïve adipocytes (Fig. 1a). Similar studies in human support this notion as well [36]. Thus, chronic IH mimicking the oscillations in oxygenation that occur in sleep apnea (as well as in other respiratory disorders) leads to major alterations of a putative GM-circulating exosome pathway that ultimately disrupts adipocyte homeostasis, resulting in metabolic dysfunction, as reflected by IR. Moreover, we show that exercise corresponding to current guidelines of regular non-strenuous activity [68] will lead to substantial improvements in the GM-exosome pathway. Thus, we propose that novel therapeutic approaches targeting the GM in OSA while encouraging regular exercise may reverse the heightened cardiometabolic risk associated with this highly prevalent disorder [5, 69].

Our findings showing increases in IR and in vWAT M1 macrophages in mice exposed to IH along with improvements by PA, indicate that the vWAT may play a central role in metabolic regulation, and that chronic-low grade inflammation in vWAT is a key process in the emergence of IR [43]. Furthermore, clinical reports in untreated OSA patients have shown progressive worsening of IR, and the emergence of the metabolic syndrome with OSA severity, independent of obesity [70-73]. Indeed, obesity is one of the major risk factors for the occurrence of OSA. Yet, the confounding roles of obesity and OSA would be difficult to extricate, and therefore our initial efforts were conducted in non-obese mice. There is no doubt that future studies will need to incorporate obese mice, and address the combination of obesity and sleep apnea to further understand the independent and inter-dependent relationships in the context of human disease. We should also emphasize that in addition to OSA, other disorders such as asthma, chronic obstructive pulmonary disease (COPD), interstitial lung disease, idiopathic pulmonary fibrosis, and restrictive lung disease characteristically exhibit diurnal oscillations in oxygenation, and intermittent hypoxia is most likely to manifest during the sleep period, thereby potentially expanding the scope of our findings to many other relevant medical conditions. Of note, decreased insulin sensitivity has been reported in healthy volunteers, lean mice, and cultured adipocytes exposed to IH [72-74]. IH also leads to other vWAT changes such as gene expression modifications, alteration in lipoprotein clearance pathways, and vascular rarefaction [8, 42, 75], all of which play a central role in metabolic regulation and emergence of IR [8, 9, 41, 43]. However, the mechanistic processes by which the IH-induced metabolic derangements both systemically and in vWAT were generated was unclear. The ever expanding extant literature clearly indicates that the GM influences multiple metabolic process in liver, intestine, brain, skeletal muscle, and vWAT [76-79], and that specific alterations in GM foster the development and progression of metabolic and cardiovascular diseases, as well as obesity [78, 80, 81]. Multiple elements within the GM have been linked to adiposity, insulin sensitivity, and glucose metabolism [82, 83]; more particularly,

Firmicutes and Bacteroidetes, have been implicated in the control of host energy metabolism including carbohydrate, lipid, and bile acid metabolism [84, 85]. Gram-positive Firmicutes (GPF) and Gram-negative Bacteroidetes (GNB) predominate in the GM, and inequality in the Firmicutes/Bacteroidetes ratio has been related to inflammatory and immune function disorders, obesity, and metabolic disease [86, 87]. We found a subset of OTUs to be enhanced in the setting of IH comprising taxa within the Gram-negative *Bacteroidetes* phylum, including *Bacteroides* sp., *Parabacteroides* sp., *Muribaculum* sp., and *Rikenella* sp.; *Lactobacillus* sp. as the sole member of the Firmicutes; and unresolved  $\alpha$ -*Proteobacteria* within the *Rhodospirillales* order. In contrast, the normoxic mice harbored significantly greater relative abundance of multiple taxa within the largely GPF phylum, including several *Lachnospiraceae* and *Ruminococcaceae*, which are associated with short- and long-chain fatty acid metabolism. *Lactobacillus* and *Clostridium* species are associated with IR [88], and higher Firmicutes-to-Bacteroidetes ratios were observed in obese children when compared to normal weight children [89, 90]. Thus, alterations in GM as induced by episodic changes in blood oxygen content are of metabolic relevance, and their reversibility may be facilitated by targeted interventions in the GM [86, 91, 92] that aim at the alterations in microbiome diversity (richness, Shannon diversity, and inverse Simpson diversity) and metabolomic complexity, along with exercise. In healthy animals, exercise was found to alter the microbiota taxonomic composition [93, 94], and exercise training also modified GM in normal and diabetic mice [95].

The decreased levels of malonic acid in IH-exposed mice are of interest, since the co-enzyme A-derivative, malonyl-CoA, plays a key role in elongation of fatty acids (FAs) in FA synthesis. The levels of malonic acid are determined by the relative rates of production (controlled by acetyl-CoA carboxylase (ACC), expressed by both prokaryotic and host cells) and consumption due to FA synthesis. Thus, alternative interpretations of the decreased levels of malonic acid in IH-exposed mice include decreased production due to reduced ACC activity or acetyl-CoA substrate, and increased use and assimilation into fatty acid synthesis. The presence of so many very long chain FAs (VLCFAs) detected via LCMS in samples from IH-exposed mice would suggest the former is more likely than the latter, although the possible explanations are not mutually exclusive and are speculative. Two nonpolar compounds detected via GCMS included hexadecanoic (C:17) acid and pentadecanoic (C:15) acid. Hexadecanoic acid is of particular relevance due to its previous associations with IH in two knock-out mouse models of atherosclerosis [96]. The elevation of C15:0 and C17:0 is viewed as a metabolic risk factor [97], and both C15:0 and C17:0 are increased in differentiated adipocytes 3T3 cells compared non differentiated cells [98]. However, pentadecanoic acid is also a FA component of several bacterial cell walls [99], and the fact that a large proportion of the FA content of feces is not traceable to the diet makes differences in groups receiving the same chow likely attributable to differences in GM-mediated production or release. Alternatively, the increased levels may be due to decreased uptake or even active secretion in to the lumen of the GI tract by the host as a component of the increased lipolysis, circulating free fatty acids (FFAs) [100], and lipotoxicity associated with IH-induced metabolic dysfunction [101]. Thus, our current work shows both gut microbial and metabolomic content are altered in IH-exposed mice and appear to impair gut function via increases in colonic epithelial permeability, and potentially via bacterial translocation, in light of the IH-induced decreases in tight junction integrity and the increases in LPS plasma levels. Moreover, regular PA significantly ameliorates these IH-induced changes.

The influence of GM on metabolic homeostasis has emerged in recent years. Intestinal *Bacteroides* strains directly modulate gut function, and transferability of insulin resistance phenotypes can be readily accomplished through FMT [86, 91, 92, 102, 103]. FMT from human healthy non-obese donors to obese patients with IR leads to

improved whole-body insulin sensitivity in the recipients [22, 23]. Transplantation of FMT from obese mice fed on high-fat diets (HFD) into germ-free recipients significantly increases adiposity when compared to transplantation of a lean microbiota [104]. As illustrated by our FMT experiments in the present study, reconstitution of IH-induced changes in naïve mice unexposed to IH resulted in the emergence of IR, thereby attesting to the GM contributions in OSA-associated metabolic risk.

This study allowed us to explore two fundamental questions: first, whether intermittent hypoxia alters gut microbiome. We posit that the alterations in gut microbial communities induced by IH are operationally involved in promoting adiposity in humans and in animal models via greater energy harvest and regulation of host energy metabolism at a supra-organismal level [105]. Gut microbiota play a key role in the metabolism of dietary precursors, including lipids, cholesterol, and choline, and changes in GM may impact the cardio-metabolic health of the host [106]. Since, OSA is characterized by episodic changes in oxygen content in gut lumen and in fecal material, so gut microbial communities will be affected, as previously shown [24]. However, it is also likely that the alterations in GM in IH-exposed mice could also be due, at least in part, to recruitment of host immune pathways triggered by intermittent hypoxia that may then modify GM. IH increased the  $\alpha$ -diversity of GM, and more specifically, promoted higher abundance of Firmicutes and a reduced abundance of Bacteroidetes and Proteobacteria phyla than normoxic controls, suggesting the possibility that physiological interplays between host and GM could be deregulated in OSA patients (see Fig. 7). We cannot exclude the possibility that GM changes were reflective of altered feeding patterns. Indeed, dietary changes can modify the gut microbiome. Conversely, changes in GM can change overall food consumption. Both of these possibilities merit further investigation.

A remarkable finding in this study is that despite a minor, albeit significant weight loss in IH-exposed mice, these mice developed insulin resistance, while exposures to sustained hypoxia of similar magnitude actually potentiate insulin sensitivity [42]. As previously mentioned, the interactions between obesity and IH remain to be explored and will be the focus of future research.

We have recently shown that plasma exosomes in patients with OSA alter naïve adipocyte insulin sensitivity [36, 107]. Notwithstanding the causal link between GM and metabolic disorders, the potential role of GM in altering circulating exosomal cargo, which then operates as the intermediate effector of the IH-induced increases in IR [51] was previously unexplored. The interaction between gut microbiota and the host involves a complex network of signaling pathways [108]. Alterations in microbiota as observed in the IH-exposed mice could be due to systemic immune pathways initially triggered by IH in the host that would then induce GM changes. Alternatively, IH would directly modify GM and its metabolic products, as suggested by the increase in the diversity observed in the bacterial communities of the fecal microbiota of mice exposed to realistic simulation of the IH that characterizes OSA [24], and then increased permeability of the gut induced by such GM changes would elicit activation of the immune response and ultimately the changes in exosomal cargo that effect systemic insulin sensitivity. Our study does not answer which of these two specific scenarios is operationally involved in current findings, and such issues will have to be addressed in future studies. Disruptions in the immune system cause dysfunction of gut barrier that results in the translocation of gut microbiota or their products through the gut epithelium [109, 110]. In a setting of IH-induced gut dysbiosis, EVs production and cargo may change and influence host signaling pathways [111]. Furthermore, EVs can regulate the microbial environment and the immune response of the host by promoting tight junction functionality and reducing exacerbated inflammatory reactions through TLR signaling [112]. Physical inactivity can increase the risk for various non

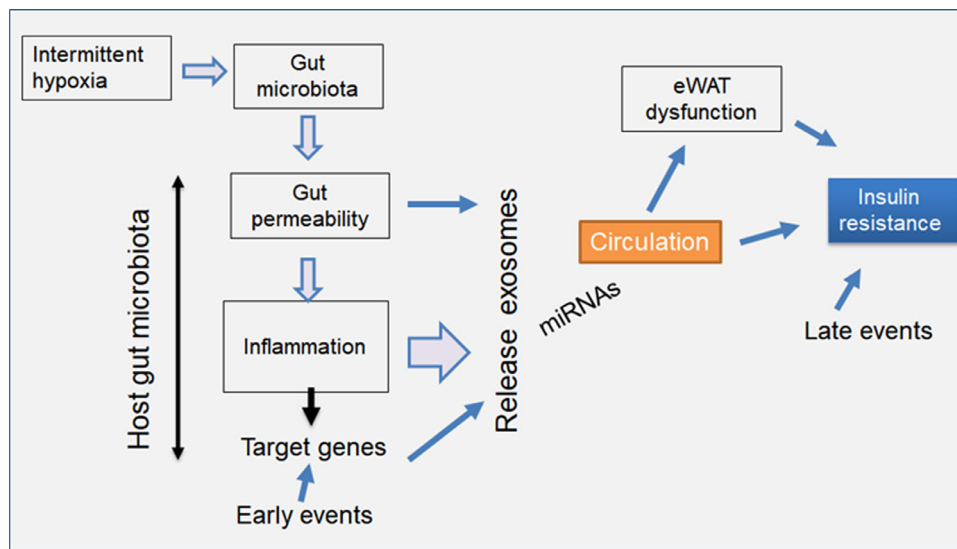


**Fig. 7.** Schematic illustrating the hypothetical bidirectional interactions between gut microbiota and exosomes in mice exposed to IH, ultimately leading to eWAT dysfunction and insulin resistance.

communicable diseases through its links to obesity in general, and more specifically in the context of excessive and inflamed vWAT [113, 114]. Interestingly, physical inactivity also increases exosomes levels in association with worsening of insulin resistance and endothelial dysfunction [115]. Conversely, exosomes may play critical roles in the crosstalk between exercise and energy homeostasis [116]. Thus, the improvements associated with PA in both GM changes and exosome cargo and function induced by IH are compatible with the putative GM-exosome pathway. The FMT experimental findings further lend supportive evidence to such contention.

It is now firmly established that the GM is altered in both animals and in humans with metabolic dysfunction, but which and how GM alterations contribute to the pathogenesis of metabolic disease including the metabolic morbidity of OSA remain unexplored. We believe the mechanistic link between GM host and exosomes is likely bidirectional. Our data show that both IH and FMT induce IR systemically and in naïve adipocytes, the latter via exposure to exosomes. The exact mechanism of how IH or FMT leads to gut permeability and to the release of exosomes into the circulation is unclear. However, we surmise that IH leads to changes in the GM by altering miRNAs in gut lumen and mRNA gene expression in colonic epithelium causing gut permeability increases and inflammation, and reciprocally, changes in immune cells in the gut wall and in circulation may promote changes in gut permeability as well. Thus, both GM alterations lead to exosomes in the circulation with a different cargo and add to the systemic effects of on end-organs such as the eWAT to induce IR (Fig. 7). The exact pathways and mechanisms through which specific signature changes in the GM induced by IH lead to the generation and release of exosomes with a functionally altered cargo are not within the scope of the current work, but is clearly of therapeutic relevance, whereby future specific manipulations of the GM may enable prevention of end-organ morbidities associated with OSA.

As limitations of this study, it is important to emphasize that we have not identified which components of the exosomal cargo that were altered by IH underlie the effects on IR. Similarly, we have not isolated and refined which GM changes are responsible for the changes in gut permeability or underlie the generation of modified exosomal cargo that accounts for IR. Independently, since exosomes carry highly complex cargo including miRNA, mRNA, lipids, proteins, and DNA, such efforts will have to be pursued in the future using multi-Omic approaches. Also, we have yet to explore non-obese and obese human subjects with and without OSA.

In conclusion, IH exposures mimicking OSA in lean mice result in consistent and recognizable changes in the GM, increased gut permeability, and altered plasma exosome cargo, the latter seemingly operating as the effector of OSA-induced IR as illustrated by the FMT experiments. The effects of IH on the GM-exosomal pathway induce systemic and white adipose tissue IR, and these alterations are ameliorated by PA. Thus, the homeostatic relationships between host and gut microbiota are likely compromised in OSA patients, and OSA-associated metabolic morbidities may benefit from not only lifestyle changes such as those afforded by PA [117], but also from other GM-targeted interventions, possibly consisting of pre- and probiotics or specific dietary manipulations [118-120].

### Contributors

DG and AK delineated the study conception and design, supervised the study, wrote the manuscript and approved the final version for publication. AE participated in microbiome experiments and analysis. RF and IA provided input on data analysis and interpretation as well as in drafting of the manuscript. ZQ conducted experiments and data analysis. All authors have read and approved the final version of the manuscript.

### Declaration of Competing Interests

The authors have no conflicts of interest to declare.

### Acknowledgment

This study was supported by grants from the National Institutes of Health grants HL130984 and HL140548 and University of Missouri Tier 2 grant. The study has not received any funding or grants from pharmaceutical or other industrial corporations. The study has not received any funding or grants from pharmaceutical or other industrial corporations.

Data Sharing: SubmissionID: SUB8478527

BioProject ID: PRJNA675081

<http://www.ncbi.nlm.nih.gov/bioproject/675081>

## Supplementary materials

Supplementary material associated with this article can be found, in the online version, at doi:10.1016/j.ebiom.2021.103208.

## References

- [1] Ryan S, Arnaud C, Fitzpatrick SF, Gaucher J, Tamisier R, Pepin JL. Adipose tissue as a key player in obstructive sleep apnoea. *Eur Respir Rev* 2019;28(152).
- [2] Khalyfa A, Kheirandish-Gozal L, Gozal D. Circulating exosomes in obstructive sleep apnea as phenotypic biomarkers and mechanistic messengers of end-organ morbidity. *Respir Physiol Neurobiol* 2018;256:143–56.
- [3] Sforza E, Roche F. Chronic intermittent hypoxia and obstructive sleep apnea: an experimental and clinical approach. *Hypoxia (Auckl)* 2016;4:99–108.
- [4] Amaddeo A, de Sanctis L, Olmo Arroyo J, Giordanella JP, Monteyrol PJ, Fauroux B. [Obesity and obstructive sleep apnea in children]. *Arch Pediatr* 2017;24(Suppl 1):S34–S8.
- [5] Mokhlesi B, Ham SA, Gozal D. The effect of sex and age on the comorbidity burden of OSA: an observational analysis from a large nationwide US health claims database. *Eur Respir J* 2016;47(4):1162–9.
- [6] Tudorache V, Traila D, Marc M, Oancea C, Manolescu D, Tudorache E, et al. Impact of moderate to severe obstructive sleep apnea on the cognition in idiopathic pulmonary fibrosis. *PLoS ONE* 2019;14(2):e0211455.
- [7] Beaudin AE, Waltz X, Hanly PJ, Poulin MJ. Impact of obstructive sleep apnoea and intermittent hypoxia on cardiovascular and cerebrovascular regulation. *Exp Physiol* 2017;102(7):743–63.
- [8] Gharib SA, Khalyfa A, Abdelkarim A, Ramesh V, Buazza M, Kaushal N, et al. Intermittent hypoxia activates temporally coordinated transcriptional programs in visceral adipose tissue. *J Mol Med* 2012;90(4):435–45.
- [9] Gozal D, Gileles-Hillel A, Cortese R, Li Y, Almendros I, Qiao Z, et al. Visceral White Adipose Tissue Following Chronic Intermittent and Sustained Hypoxia in Mice. *Am J Respir Cell Mol Biol* 2017.
- [10] Ryan S. Adipose tissue inflammation by intermittent hypoxia: mechanistic link between obstructive sleep apnoea and metabolic dysfunction. *J Physiol* 2017;595(8):2423–30.
- [11] Heiss CN, Olofsson LE. Gut microbiota-dependent modulation of energy metabolism. *J Innate Immun* 2018;10(3):163–71.
- [12] Gopalakrishnan V, Helmink BA, Spencer CN, Reuben A, Wargo JA. The influence of the gut microbiome on cancer, immunity, and cancer immunotherapy. *Cancer Cell* 2018;33(4):570–80.
- [13] Levy M, Kolodziejczyk AA, Thaiss CA, Elinav E. Dysbiosis and the immune system. *Nat Rev Immunol* 2017;17(4):219–32.
- [14] Iaccarino G, Franco D, Sorriento D, Strisciuglio T, Barbato E, Morisco C. Modulation of insulin sensitivity by exercise training: implications for cardiovascular prevention. *J Cardiovasc Transl Res* 2020.
- [15] Headid Iii RJ, Park SY. The impacts of exercise on pediatric obesity. *Clin Exp Pediatr* 2020.
- [16] Sirico F, Bianco A, D'Alicandro G, Castaldo C, Montagnani S, Spera R, et al. Effects of physical exercise on adiponectin, leptin, and inflammatory markers in childhood obesity: systematic review and meta-analysis. *Child Obes* 2018;14(4):207–17.
- [17] Whooten R, Kerem L, Stanley T. Physical activity in adolescents and children and relationship to metabolic health. *Curr Opin Endocrinol Diabetes Obes* 2019;26(1):25–31.
- [18] Garcia-Hermoso A, Saavedra JM, Escalante Y, Sanchez-Lopez M, Martinez-Vizcaino V. Endocrinology and Adolescence: aerobic exercise reduces insulin resistance markers in obese youth: a meta-analysis of randomized controlled trials. *Eur J Endocrinol* 2014;171(4):R163–71.
- [19] Sohail MU, Yassine HM, Sohail A, Al Thani AA. Impact of physical exercise on gut microbiome, inflammation, and the pathobiology of metabolic disorders. *Rev Diabet Stud* 2019;15:35–48.
- [20] Ussar S, Fujisaka S, Kahn CR. Interactions between host genetics and gut microbiome in diabetes and metabolic syndrome. *Mol Metab* 2016;5(9):795–803.
- [21] Kelly CR, Ihunnah C, Fischer M, Khoruts A, Surawicz C, Afzali A, et al. Fecal microbiota transplant for treatment of *Clostridium difficile* infection in immunocompromised patients. *Am J Gastroenterol* 2014;109(7):1065–71.
- [22] Kootte RS, Levin E, Salojarvi J, Smits LP, Hartstra AV, Udayappan SD, et al. Improvement of insulin sensitivity after lean donor feces in metabolic syndrome is driven by baseline intestinal microbiota composition. *Cell Metab* 2017;26(4):611–9 e6.
- [23] Vrieze A, Van Nood E, Holleman F, Salojarvi J, Kootte RS, Bartelsman JF, et al. Transfer of intestinal microbiota from lean donors increases insulin sensitivity in individuals with metabolic syndrome. *Gastroenterology* 2012;143(4):913–6 e7.
- [24] Moreno-Indias I, Torres M, Montserrat JM, Sanchez-Alcoholado L, Cardona F, Tinahones FJ, et al. Intermittent hypoxia alters gut microbiota diversity in a mouse model of sleep apnoea. *Eur Respir J* 2015;45(4):1055–65.
- [25] Farre N, Farre R, Gozal D. Sleep apnea morbidity: a consequence of microbial-immune cross-talk? *Chest* 2018;154(4):754–9.
- [26] Poroyko VA, Carreras A, Khalyfa A, Khalyfa AA, Leone V, Peris E, et al. Chronic sleep disruption alters gut microbiota, induces systemic and adipose tissue inflammation and insulin resistance in mice. *Sci Rep* 2016;6:35405.
- [27] Badran M, Khalyfa A, Ericsson A, Gozal D. Fecal microbiota transplantation from mice exposed to chronic intermittent hypoxia elicits sleep disturbances in naive mice. *Exp Neurol* 2020;334:113439.
- [28] Li J, Zhou C, Li J, Su Z, Sang H, Jia E, et al. Global correlation analysis for microRNA and gene expression profiles in human obesity. *Pathol Res Pract* 2015;211(5):361–8.
- [29] Mathieu M, Martin-Jaular L, Lavieu G, Thery C. Specificities of secretion and uptake of exosomes and other extracellular vesicles for cell-to-cell communication. *Nat Cell Biol* 2019;21(1):9–17.
- [30] Khalyfa A, Kheirandish-Gozal L, Khalyfa AA, Philby MF, Alonso-Alvarez ML, Mohammadi M, et al. Circulating plasma extracellular microvesicle microrna cargo and endothelial dysfunction in children with obstructive sleep apnea. *Am J Respir Crit Care Med* 2016;194(9):1116–26.
- [31] Colombo M, Raposo G, Thery C. Biogenesis, secretion, and intercellular interactions of exosomes and other extracellular vesicles. *Annu Rev Cell Dev Biol* 2014;30:255–89.
- [32] Zhao H, Shang Q, Pan Z, Bai Y, Li Z, Zhang H, et al. Exosomes from adipose-derived stem cells attenuate adipose inflammation and obesity through polarizing M2 macrophages and being in white adipose tissue. *Diabetes* 2018;67(2):235–47.
- [33] Vlassov AV, Magdaleno S, Setterquist R, Conrad R. Exosomes: current knowledge of their composition, biological functions, and diagnostic and therapeutic potentials. *Biochim Biophys Acta* 2012;1820(7):940–8.
- [34] Lotvall J, Hill AF, Hochberg F, Buzas EI, Di Vizio D, Gardiner C, et al. Minimal experimental requirements for definition of extracellular vesicles and their functions: a position statement from the International Society for Extracellular Vesicles. *J Extracell Vesicles* 2014;3:26913.
- [35] Thery C, Witwer KW, Aikawa E, Alcaraz MJ, Anderson JD, Andriantsitohaina R, et al. Minimal information for studies of extracellular vesicles 2018 (MISEV2018): a position statement of the international society for extracellular vesicles and update of the MISEV2014 guidelines. *J Extracell Vesicles* 2018;7(1):1535750.
- [36] Khalyfa A, Gozal D, Masa JF, Marin JM, Qiao Z, Corral J, et al. Sleep-disordered breathing, circulating exosomes, and insulin sensitivity in adipocytes. *Int J Obes* 2018;42(6):1127–39.
- [37] Pan J, Alimujiang M, Chen Q, Shi H, Luo X. Exosomes derived from miR-146a-modified adipose-derived stem cells attenuate acute myocardial infarction-induced myocardial damage via downregulation of early growth response factor 1. *J Cell Biochem* 2019;120(3):4433–43.
- [38] Deng ZB, Poliakov A, Hardy RW, Clements R, Liu C, Liu Y, et al. Adipose tissue exosome-like vesicles mediate activation of macrophage-induced insulin resistance. *Diabetes* 2009;58(11):2498–505.
- [39] Safdar A, Saleem A, Tamopolsky MA. The potential of endurance exercise-derived exosomes to treat metabolic diseases. *Nat Rev Endocrinol* 2016;12(9):504–17.
- [40] Gozal D, Nair D, Goldbart AD. Physical activity attenuates intermittent hypoxia-induced spatial learning deficits and oxidative stress. *Am J Respir Crit Care Med* 2010;182(1):104–12.
- [41] Khalyfa A, Qiao Z, Gileles-Hillel A, Khalyfa AA, Akbarpour M, Popko B, et al. Activation of the integrated stress response and metabolic dysfunction in a murine model of sleep apnea. *Am J Respir Cell Mol Biol* 2017;57(4):477–86.
- [42] Gozal D, Gileles-Hillel A, Cortese R, Li Y, Almendros I, Qiao Z, et al. Visceral white adipose tissue after chronic intermittent and sustained hypoxia in mice. *Am J Respir Cell Mol Biol* 2017;56(4):477–87.
- [43] Gileles-Hillel A, Almendros I, Khalyfa A, Nigdelioglu R, Qiao Z, Hamanaka RB, et al. Prolonged exposures to intermittent hypoxia promote visceral white adipose tissue inflammation in a murine model of severe sleep apnea: effect of normoxic recovery. *Sleep* 2017;40(3).
- [44] Farre R, Montserrat JM, Gozal D, Almendros I, Navajas D. Intermittent hypoxia severity in animal models of sleep apnea. *Front Physiol* 2018;9:1556.
- [45] Mutskov V, Khalyfa A, Wang Y, Carreras A, Nobrega MA, Gozal D. Early-life physical activity reverses metabolic and Foxo1 epigenetic misregulation induced by gestational sleep disturbance. *Am J Physiol Regul Integr Comp Physiol* 2015;308(5):R419–30.
- [46] Gozal D, Qiao Z, Almendros I, Zheng J, Khalyfa A, Shimpukade B, et al. Treatment with TUG891, a free fatty acid receptor 4 agonist, restores adipose tissue metabolic dysfunction following chronic sleep fragmentation in mice. *Int J Obes* 2016;40(7):1143–9.
- [47] Khalyfa A, Carreras A, Almendros I, Hakim F, Gozal D. Sex dimorphism in late gestational sleep fragmentation and metabolic dysfunction in offspring mice. *Sleep* 2015;38(4):545–57.
- [48] Khalyfa A, Carreras A, Hakim F, Cunningham JM, Wang Y, Gozal D. Effects of late gestational high-fat diet on body weight, metabolic regulation and adipokine expression in offspring. *Int J Obes* 2013;37(11):1481–9.
- [49] Khalyfa A, Mutskov V, Carreras A, Khalyfa AA, Hakim F, Gozal D. Sleep fragmentation during late gestation induces metabolic perturbations and epigenetic changes in adiponectin gene expression in male adult offspring mice. *Diabetes* 2014;63(10):3230–41.
- [50] Stebbeg M, Silva-Cayetano A, Innocentin S, Jenkins TP, Cantacessi C, Gilbert C, et al. Heterochronic faecal transplantation boosts gut germinal centres in aged mice. *Nat Commun* 2019;10(1):2443.
- [51] Khalyfa A, Poroyko VA, Qiao Z, Gileles-Hillel A, Khalyfa AA, Akbarpour M, et al. Exosomes and metabolic function in mice exposed to alternating dark-light cycles mimicking night shift work schedules. *Front Physiol* 2017;8:882.
- [52] Johnson PJ, Hargreaves LL, Zobrist CN, Ericsson AC. Utility of a portable desiccant system for preservation of fecal samples for downstream 16S rRNA amplicon sequencing. *J Microbiol Methods* 2018;146:1–6.
- [53] Walters WA, Caporaso JG, Lauber CL, Berg-Lyons D, Fierer N, Knight R. Primer-Prospector: de novo design and taxonomic analysis of barcoded polymerase chain reaction primers. *Bioinformatics* 2011;27(8):1159–61.

- [54] Caporaso JG, Lauber CL, Walters WA, Berg-Lyons D, Lozupone CA, Turnbaugh PJ, et al. Global patterns of 16S rRNA diversity at a depth of millions of sequences per sample. *Proc Natl Acad Sci U S A* 2011;108(Suppl 1):4516–22.
- [55] Magoc T, Salzberg SL. FLASH: fast length adjustment of short reads to improve genome assemblies. *Bioinformatics* 2011;27(21):2957–63.
- [56] Edgar RC. Search and clustering orders of magnitude faster than BLAST. *Bioinformatics* 2010;26(19):2460–1.
- [57] Pruesse E, Quast C, Knittel K, Fuchs BM, Ludwig W, Peplies J, et al. SILVA: a comprehensive online resource for quality checked and aligned ribosomal RNA sequence data compatible with ARB. *Nucleic Acids Res* 2007;35(21):7188–96.
- [58] Deda O, Chatziioannou AC, Fasoula S, Palachanis D, Raikos N, Theodoridis GA, et al. Sample preparation optimization in fecal metabolic profiling. *J Chromatogr B Analyt Technol Biomed Life Sci* 2017;1047:115–23.
- [59] Lei Z, Sumner BW, Bhatia A, Sarma SJ, Sumner LW. UHPLC-MS analyses of plant flavonoids. *Curr Protoc Plant Biol* 2019;4(1):e20085.
- [60] Vu DC, Lei ZT, Sumner LW, Coggshall MV, Lin CH. Identification and quantification of phytochemicals in black walnut kernels. *J Food Compos Anal* 2019;75:61–9.
- [61] Vieira-Potter VJ, Cross TWL, Swanson KS, Sarma SJ, Lei ZT, Sumner LW, et al. Soy-induced fecal metabolome changes in ovariectomized and intact female rats: relationship with cardiometabolic health. *Sci Rep* 2018;8:12.
- [62] Trzepizur W, Khalyfa A, Qiao Z, Popko B, Gozal D. Integrated stress response activation by sleep fragmentation during late gestation in mice leads to emergence of adverse metabolic phenotype in offspring. *Metabolism* 2017.
- [63] Khalyfa A, Almendros I, Gileles-Hillel A, Akbarpour M, Trzepizur W, Mokhlesi B, et al. Circulating exosomes potentiate tumor malignant properties in a mouse model of chronic sleep fragmentation. *Oncotarget* 2016;7(34):54676–90.
- [64] Khalyfa A, Khalyfa AA, Akbarpour M, Connes P, Romana M, Lapping-Carr G, et al. Extracellular microvesicle microRNAs in children with sickle cell anaemia with divergent clinical phenotypes. *Br J Haematol* 2016;174(5):786–98.
- [65] Khalyfa A, Zhang C, Khalyfa AA, Foster GE, Beaudin AE, Andrade J, et al. Effect on intermittent hypoxia on plasma exosomal micro RNA signature and endothelial function in healthy adults. *Sleep* 2016;39(12):2077–90.
- [66] Almendros I, Khalyfa A, Trzepizur W, Gileles-Hillel A, Huang L, Akbarpour M, et al. Tumor cell malignant properties are enhanced by circulating exosomes in sleep apnea. *Chest* 2016;150(5):1030–41.
- [67] Øyvind H, Harper ATD, Ryan DP. Past: paleontological statistics software package for education and data analysis. *Paleontol Electron* 2001;4(1):1.
- [68] Smith Jr. SC, Allen J, Blair SN, Bonow RO, Brass LM, Fonarow GC, et al. AHA/ACC guidelines for secondary prevention for patients with coronary and other atherosclerotic vascular disease: 2006 update: endorsed by the national heart, lung, and blood institute. *Circulation* 2006;113(19):2363–72.
- [69] Gileles-Hillel A, Kheirandish-Gozal L, Gozal D. Biological plausibility linking sleep apnoea and metabolic dysfunction. *Nat Rev Endocrinol* 2016;12(5):290–8.
- [70] Priou P, Le Vaillant M, Meslier N, Chollet S, Masson P, Humeau MP, et al. Independent association between obstructive sleep apnea severity and glycated hemoglobin in adults without diabetes. *Diabetes Care* 2012;35(9):1902–6.
- [71] Pamidi S, Wroblewski K, Broussard J, Day A, Hanlon EC, Abraham V, et al. Obstructive sleep apnea in young lean men: impact on insulin sensitivity and secretion. *Diabetes Care* 2012;35(11):2384–9.
- [72] Soin D, Kumar PA, Chahal J, Chawla SPS, Kaur S, Garg R, et al. Evaluation of obstructive sleep apnea in metabolic syndrome. *J Family Med Prim Care* 2019;8(5):1580–6.
- [73] Hirotsu C, Haba-Rubio J, Togeiro SM, Marques-Vidal P, Drager LF, Vollenweider P, et al. Obstructive sleep apnoea as a risk factor for incident metabolic syndrome: a joined Episono and HypnoLaus prospective cohorts study. *Eur Respir J* 2018;52(5).
- [74] Murphy AM, Thomas A, Crinion SJ, Kent BD, Tambuwala MM, Fabre A, et al. Intermittent hypoxia in obstructive sleep apnoea mediates insulin resistance through adipose tissue inflammation. *Eur Respir J* 2017;49(4).
- [75] Yao Q, Shin MK, Jun JC, Hernandez KL, Aggarwal NR, Mock JR, et al. Effect of chronic intermittent hypoxia on triglyceride uptake in different tissues. *J Lipid Res* 2013;54(4):1058–65.
- [76] Braniste V, Al-Asmakh M, Kowal C, Anuar F, Abbaspour A, Toth M, et al. The gut microbiota influences blood-brain barrier permeability in mice. *Sci Transl Med* 2014;6(263):263ra158.
- [77] Montagner A, Korecka A, Polizzi A, Lippi Y, Blum Y, Canlet C, et al. Hepatic circadian clock oscillators and nuclear receptors integrate microbiome-derived signals. *Sci Rep* 2016;6:20127.
- [78] Lahiri S, Kim H, Garcia-Perez I, Reza MM, Martin KA, Kundu P, et al. The gut microbiota influences skeletal muscle mass and function in mice. *Sci Transl Med* 2019;11(502).
- [79] Virtue AT, McCrigh SJ, Wright JM, Jimenez MT, Mowle WK, Kotzin JJ, et al. The gut microbiota regulates white adipose tissue inflammation and obesity via a family of microRNAs. *Sci Transl Med* 2019;11(496).
- [80] Battson ML, Lee DM, Weir TL, Gentile CL. The gut microbiota as a novel regulator of cardiovascular function and disease. *J Nutr Biochem* 2018;56:1–15.
- [81] Sharma S, Tripathi P. Gut microbiome and type 2 diabetes: where we are and where to go? *J Nutr Biochem* 2019;63:101–8.
- [82] Backhed F, Ding H, Wang T, Hooper LV, Koh GY, Nagy A, et al. The gut microbiota as an environmental factor that regulates fat storage. *Proc Natl Acad Sci U S A* 2004;101(44):15718–23.
- [83] Ley RE, Backhed F, Turnbaugh P, Lozupone CA, Knight RD, Gordon JL. Obesity alters gut microbial ecology. *Proc Natl Acad Sci U S A* 2005;102(31):11070–5.
- [84] Turnbaugh PJ, Ley RE, Mahowald MA, Magrini V, Mardis ER, Gordon JL. An obesity-associated gut microbiome with increased capacity for energy harvest. *Nature* 2006;444(7122):1027–31.
- [85] Swann JR, Want EJ, Geier FM, Spagou K, Wilson ID, Sidaway JE, et al. Systemic gut microbial modulation of bile acid metabolism in host tissue compartments. *Proc Natl Acad Sci U S A* 2011;108(Suppl 1):4523–30.
- [86] Singh RK, Chang HW, Yan D, Lee KM, Ucmak D, Wong K, et al. Influence of diet on the gut microbiome and implications for human health. *J Transl Med* 2017;15(1):73.
- [87] Boulange CL, Neves AL, Chilloux J, Nicholson JK, Dumas ME. Impact of the gut microbiota on inflammation, obesity, and metabolic disease. *Genome Med* 2016;8(1):42.
- [88] Karlsson FH, Tremaroli V, Nookaew I, Bergstrom G, Behre CJ, Fagerberg B, et al. Gut metagenome in European women with normal, impaired and diabetic glucose control. *Nature* 2013;498(7452):99–103.
- [89] Riva A, Borgo F, Lassandro C, Verduci E, Morace G, Borghi E, et al. Pediatric obesity is associated with an altered gut microbiota and discordant shifts in Firmicutes populations. *Environ Microbiol* 2017;19(1):95–105.
- [90] Bervoets L, Van Hoorenbeeck K, Kortleven I, Van Noten C, Hens N, Vael C, et al. Differences in gut microbiota composition between obese and lean children: a cross-sectional study. *Gut Pathog* 2013;5(1):10.
- [91] Cresci GA, Bowden E. Gut Microbiome: what We Do and Don't Know. *Nutr Clin Pract* 2015;30(6):734–46.
- [92] Milani C, Duranti S, Bottacini F, Casey E, Turroni F, Mahony J, et al. The first microbial colonizers of the human gut: composition, activities, and health implications of the infant gut microbiota. *Microbiol Mol Biol Rev* 2017;81(4).
- [93] Queipo-Ortuno MI, Seoane LM, Murri M, Pardo M, Gomez-Zumaquero JM, Cardona F, et al. Gut microbiota composition in male rat models under different nutritional status and physical activity and its association with serum leptin and ghrelin levels. *PLoS ONE* 2013;8(5):e65465.
- [94] Evans CC, LePard KJ, Kwak JW, Stancukas MC, Laskowski S, Dougherty J, et al. Exercise prevents weight gain and alters the gut microbiota in a mouse model of high fat diet-induced obesity. *PLoS ONE* 2014;9(3):e92193.
- [95] Lambert JE, Myslicki JP, Bomhof MR, Belke DD, Shearer J, Reimer RA. Exercise training modifies gut microbiota in normal and diabetic mice. *Appl Physiol Nutr Metab* 2015;40(7):749–52.
- [96] Millar CL, Norris GH, Vitals A, Garcia C, Seibel S, Anto L, et al. Dietary egg sphingomyelin prevents aortic root plaque accumulation in apolipoprotein-E knockout mice. *Nutrients* 2019;11(5).
- [97] Matthan NR, Ooi EM, Van Horn L, Neuhouser ML, Woodman R, Lichtenstein AH. Plasma phospholipid fatty acid biomarkers of dietary fat quality and endogenous metabolism predict coronary heart disease risk: a nested case-control study within the Women's Health Initiative observational study. *J Am Heart Assoc* 2014;3(4).
- [98] Roberts LD, Virtue S, Vidal-Puig A, Nicholls AW, Griffin JL. Metabolic phenotyping of a model of adipocyte differentiation. *Physiol Genom* 2009;39(2):109–19.
- [99] Li Y, Wu S, Wang L, Li Y, Shi F, Wang X. Differentiation of bacteria using fatty acid profiles from gas chromatography-tandem mass spectrometry. *J Sci Food Agric* 2010;90(8):1380–3.
- [100] Chopra S, Rathore A, Younas H, Pham LV, Gu C, Beselman A, et al. Obstructive sleep apnea dynamically increases nocturnal plasma free fatty acids, glucose, and cortisol during sleep. *J Clin Endocrinol Metab* 2017;102(9):3172–81.
- [101] Gu C, Younas H, Jun JC. Sleep apnea: an overlooked cause of lipotoxicity? *Med Hypotheses* 2017;108:161–5.
- [102] Le Chatelier E, Nielsen T, Qin J, Prifti E, Hildebrand F, Falony G, et al. Richness of human gut microbiome correlates with metabolic markers. *Nature* 2013;500(7464):541–6.
- [103] Freitas M, Tavan E, Cayuela C, Diop L, Sapin C, Trugnan G. Host-pathogens cross-talk. Indigenous bacteria and probiotics also play the game. *Biology of the cell / under the auspices of the Euro Cell Biol Organ* 2003;95(8):503–6.
- [104] Turnbaugh PJ, Backhed F, Fulton L, Gordon JL. Diet-induced obesity is linked to marked but reversible alterations in the mouse distal gut microbiome. *Cell Host Microbe* 2008;3(4):213–23.
- [105] Backhed F, Manchester JK, Semenkovich CF, Gordon JL. Mechanisms underlying the resistance to diet-induced obesity in germ-free mice. *Proc Natl Acad Sci U S A* 2007;104(3):979–84.
- [106] Garcia-Rios A, Torres-Pena JD, Perez-Jimenez F, Perez-Martinez P. Gut microbiota: a new marker of cardiovascular disease. *Curr Pharm Des* 2017;23(22):3233–8.
- [107] Khalyfa A, Kheirandish-Gozal L, Gozal D. Exosome and macrophage crosstalk in sleep-disordered breathing-induced metabolic dysfunction. *Int J Mol Sci* 2018;19(11).
- [108] Thompson JA, Oliveira RA, Djukovic A, Ubeda C, Xavier KB. Manipulation of the quorum sensing signal AI-2 affects the antibiotic-treated gut microbiota. *Cell Rep* 2015;10(11):1861–71.
- [109] Henao-Mejia J, Elinav E, Jin C, Hao L, Mehal WZ, Strowig T, et al. Inflammation-mediated dysbiosis regulates progression of NAFLD and obesity. *Nature* 2012;482(7384):179–85.
- [110] Cani PD, Osto M, Geurts L, Everard A. Involvement of gut microbiota in the development of low-grade inflammation and type 2 diabetes associated with obesity. *Gut Microbes* 2012;3(4):279–88.
- [111] Li J, Azam F, Zhang S. Outer membrane vesicles containing signalling molecules and active hydrolytic enzymes released by a coral pathogen *Vibrio shilonii* AK1. *Environ Microbiol* 2016;18(11):3850–66.
- [112] Molina-Tijeras JA, Galvez J, Rodriguez-Cabezas ME. The immunomodulatory properties of extracellular vesicles derived from probiotics: a novel approach for the management of gastrointestinal diseases. *Nutrients* 2019;11(5).
- [113] Booth FW, Roberts CK, Laye MJ. Lack of exercise is a major cause of chronic diseases. *Compr Physiol* 2012;2(2):1143–211.

- [114] Schipper HS, Prakken B, Kalkhoven E, Boes M. Adipose tissue-resident immune cells: key players in immunometabolism. *Trends Endocrinol Metab* 2012;23(8):407–15.
- [115] Navasolava NM, Dignat-George F, Sabatier F, Larina IM, Demiot C, Fortrat JO, et al. Enforced physical inactivity increases endothelial microparticle levels in healthy volunteers. *Am J Physiol Heart Circ Physiol* 2010;299(2):H248–56.
- [116] Whitham M, Parker BL, Friedrichsen M, Hingst JR, Hjorth M, Hughes WE, et al. Extracellular vesicles provide a means for tissue crosstalk during exercise. *Cell Metab* 2018;27(1):237–51 e4.
- [117] Martinez-Gomez D, Lavie CJ, Hamer M, Cabanas-Sanchez V, Garcia-Esquinas E, Pareja-Galeano H, et al. Physical activity without weight loss reduces the development of cardiovascular disease risk factors - a prospective cohort study of more than one hundred thousand adults. *Prog Cardiovasc Dis* 2019;62(6):522–30.
- [118] Mashaqi S, Gozal D. Obstructive sleep apnea and systemic hypertension: gut dysbiosis as the mediator? *J Clin Sleep Med* 2019;15(10):1517–27.
- [119] Ganesh BP, Nelson JW, Eskew JR, Ganesan A, Ajami NJ, Petrosino JF, et al. Prebiotics, probiotics, and acetate supplementation prevent hypertension in a model of obstructive sleep apnea. *Hypertension*. 2018;72(5):1141–50.
- [120] Song H, Zhang J, Qu J, Liu J, Yin P, Zhang G, et al. *Lactobacillus rhamnosus* GG microcapsules inhibit *Escherichia coli* biofilm formation in coculture. *Biotechnol Lett* 2019;41(8–9):1007–14.